An exploratory investigation of brain collateral circulation plasticity after cerebral ischemia in two experimental C57BL/6 mouse models

Marco Foddis*[1], Katarzyna Winek*[1], Kajetan Bentele[2], Susanne Mueller[1,3], Sonja Blumenau[1], Nadine Reichhart N.[4], Sergio Crespo-Garcia[4], Dermot Harnett[2], Andranik Ivanov[2], Andreas Meisel[1], Antonia Joussen[4], Olaf Strauss[4], Dieter Beule [2], Ulrich Dirnagl [1, 5°], Celeste Sassi [1]

*= equal contribution

° = corresponding author

[1]Department of Experimental Neurology, Center for Stroke Research Berlin (CSB), Charité - Universitätsmedizin Berlin, Corporate Member of Freie Universität Berlin, Humboldt-Universität zu Berlin, and Berlin Institute of Health, Berlin, Germany.

[2]Berlin Institute of Health, BIH, Unit Bioinformatics, Berlin, Germany.

[3]Charité – Universitätsmedizin Berlin, NeuroCure Cluster of Excellence and Charité Core Facility 7T Experimental MRIs

[4]Department of Ophthalmology, Experimental Ophthalmology, Charité Universitätsmedizin Berlin, Berlin, Germany.

[5]QUEST Center for Transforming Biomedical Research, Berlin Institute of Health (BIH), Berlin, Germany

Corresponding author:
Prof. Ulrich Dirnagl,
Ulrich.Dirnagl@charite.de
Department of Experimental Neurology
Charité Universitätsmedizin Berlin, Germany
Tel: +49 30 450 560134
Fax: +49 30 450 560942

Running Headline
'Brain collateral circulation in 2 mouse models'

ABSTRACT

Brain collateral circulation is an essential compensatory mechanism in response to acute brain ischemia. To study the temporal evolution of brain macro and microcollateral recruitment and their reciprocal interactions in response to different ischemic conditions, we applied a combination of complementary techniques (T2 weighted magnetic resonance imaging [MRI], time of flight [TOF] angiography [MRA], cerebral blood flow [CBF] imaging and histology) in two different mouse models. Hypoperfusion was either induced by permanent bilateral common carotid artery stenosis (BCCAS) or 60 minute transient unilateral middle cerebral artery occlusion (MCAO).

In both models, collateralization is a very dynamic phenomenon with a global effect affecting both hemispheres. Patency of ipsilateral posterior communicating artery (PcomA) represents the main variable survival mechanism and the main determinant of stroke lesion volume and recovery in MCAO whereas the promptness of external carotid artery retrograde flow recruitment together with PcomA patency, critically influence survival, brain ischemic lesion volume and retinopathy in BCCAS mice. Finally, different ischemic gradients shape microcollateral density and size.

Key words

Stroke, collateral vessels, posterior communicating arteries (PcomAs), middle cerebral artery occlusion (MCAO), bilateral common carotid artery stenosis (BCCAS).

INTRODUCTION

Collateral circulation represents an essential neuroprotective mechanism during severe acute brain ischemia-hypoxia. Despite the critical importance of collateral arteries, their clinical and neuroradiological assessment in patients remains a major challenge [1,2]. First, collateral arteries represent a complex trait, highly influenced by genetic, sex and age-related variability. Second, they are recruited exclusively under moderate-severe acute ischemic conditions like transient ischemic attack (TIA) and strokes. Third, additional cardiovascular risk factors may frequently co-exist and exert an additive effect on the ischemia outcome

(hypertension, diabetes, atherosclerosis, and aging). Finally, standardized and validated neuroimaging methods to study collateral circulation are still lacking [1,2].

By contrast, inbred mice, minimizing genetic, epigenetic and environmental factors, offer a unique window into the brain collateral circulation plasticity [3,4,5]. Nevertheless, only few studies described collateral circulation in mice, mainly focusing on posterior communicating arteries (PcomAs) and leptomeningeal arteriole variability in different mouse strains [2]. Particularly, variability in the in the extension of the collateral circulation in terms of collateral number and diameter has been reported between C57BL/6 and BALB/cByJ that display high and low extent of collaterals, respectively, resulting in significantly different infarct volumes [6].

On the other hand, intrastrain dynamic PcomA patency and the hemodynamic response of the whole brain collateral circulation to compensate PcomA variability remains largely unexplored.

This study aims to provide a comprehensive description of the macro and microcollateral artery plasticity during brain acute and subacute hypoperfusion in two experimental mouse models (MCAO and BCCAS).Therefore, we applied a combination of complementary techniques (T2 weighted magnetic resonance imaging [T2-MRI], arterial spin labeling cerebral blood flow [CBF], magneto resonance angiography [MRA] and histology) to study two C57/BL6J background brain hypoperfusion mouse models, where hypoperfusion is the result of either bilateral CCA stenosis (BCCAS) or 60 minute unilateral blockage of the left MCA with permanent occlusion of CCA and ECA (MCAO).

Our study may provide potential insights that could be translated into the clinic, both in terms of a more informed use of these experimental models and better understanding of the brain collateral circulation.

MATERIAL AND METHODS

Animals, experimental design and exclusion criteria

Experiments were approved by the Landesamt für Gesundheit und Soziales and conducted according to the German Animal Welfare Act and ARRIVE guidelines (https://www.nc3rs.org.uk/arrive-guidelines). 34 and 18 male C57/BL6 J mice (purchased at

8 weeks of age, Charles River, Germany and 10 weeks of age Janvier France, respectively) were housed in a temperature (22±2°C), humidity (55±10%), and light (12/12-hour light/dark cycle) controlled environment. The animals underwent hypoperfusion between 9 and 13 weeks of age (n=42, BCCAS= 27, MCAO= 15) or were used as controls (naïve=7; MCAO sham=3) (**FigS1 A, B**)

The only exclusion criterion was death during MRI due to wrong placement of the animal in the scanner and led to exclusion of 2 MCAO and 2 sham animals (MCAO group), resulting in final analyzed sample size of MCAO = 13 and MCAO sham =1.

BCCAS mice were imaged before surgery, 24 hours and 1 week post-surgery. The BCCAS data from 7 weeks are data from a previous study[7] focused on the same BCCAS model that we used because we sacrificed our BCCAS mice after 7 days. They are important to show that after 7 weeks, the CBF recovery is associated to a complete CoW loop detected on MRA, analogously to the pre-surgery condition. MCAO mice were imaged 24 hours, 1week, 4 weeks and 7 weeks post-surgery for angiography and estimation of cerebral blood flow (CBF) using arterial spin labeling. At 2 days and 8 days (BCCAS) and 7 weeks (MCAO) tissue was processed for immunohistochemistry

Histology

PFA perfused brains were cut into 50-µm-thick sections on a cryostat. After washing with phosphate-buffered saline (PBS), free-floating sections were incubated with 10% normal goat serum (NGS, GeneTech, GTX27481) and 0.1% Triton-X-100 (Sigma-Aldrich, X100) in PBS for 1 h at room temperature to block unspecific binding. Primary and secondary antibodies were diluted in 1% NGS and 0.1% Triton-X-100 in PBS. Sections were incubated with rat anti-GFAP primary antibody (Millipore, 345860) for astrocytes and rabbit anti-Iba-1 primary antibody (Wako Chemicals, catalog #019-19741; RRID: AB_839504) for microglia and macrophages at 4°C overnight. After thorough washing, sections were incubated at room temperature with AlexaFluor-594- conjugated goat anti-rat (anti-GFAP, Invitrogen, catalog #A11081) and AlexaFluor- 488-conjugated goat anti-rabbit (anti-Iba-1 Invitrogen, catalog #A11034) secondary antibodies for 2 h at room temperature. WGA Alexa Fluor 680 conjugate anti-lectin together with Evans Blue was used to stain blood vessels (further details in supplemental materials and methods). Nuclei were counterstained with DAPI (Fluka, 32670). Sections were

mounted with anti-fading mounting medium Shandon Immuno Mount (Thermo Scientific, 9990402) on Super Frost Plus glass slides (R.Langenbrinck, 03-0060). Microphotographs were taken with a confocal microscope (Leica TCS SPE; RRID: SciRes_000154).

Methods to prevent bias, statistics.

This is an exploratory, descriptive study. Sample sizes were not based on *a priori* power calculation. Only descriptive but no test statistic was used. Mice were randomized to receive hypoperfusion.

PcomA size

Following Martin et al. [8] , we grade the PcomA patency in hypoperfused mice, using the ratio between PcomA and basilar artery (BA) diameters. Martin and colleagues identified 4 PcomA classes in naïve mice: 1) PcomA <10% of BA; 2) PcomA 11-20% of BA; 3) PcomA 21-30% of BA and 4) PcomA >30% of BA. Although we are convinced that PcomA patency is a functional phenotype that can only be observed after PcomA recruitment, we kept the same classification for hypoperfused mice, where both PcomA and BA diameter are increased, leaving, to different extents, the PcomA/BA ratio likely similar to the one observed in naive mice. Based on our experiments, class 1 and class 2 have been detected either in naïve mice or MCAO and BCCAS mice that died few hours post-surgery, strongly arguing for a non-patent PcomA. Therefore, we identify class 1 and class 2 as ´non-patent´, class 3 as ´small ´, class 4 as ´prominent´ and introduce a fifth class, represented by PcomA>60% of BA, described as 'very prominent'.

The diameters of the PcomAs were measured at the smallest point and the diameter of the BA was measured proximal to the superior cerebellar arteries both for the Evans Blue and fluorescent WGA stainings with ImageJ. The diameter of the PcomAs as a percentage of the diameter of the BA was calculated and used in the analysis as previously described [8] (**FigS2 A, B**).

Angiotool

Vascular density, vessel length, end points, total vascular junctions and junction density were calculated for both striatal, cortical and leptomeningeal microvessels, selecting always the same regions of interest (both in terms of brain area in both hemispheres and region of

interest dimension) by using the software AngioTool v 0.6a as previously described (**FigS2 C, D**) [9]

Additional information are included in the supplementary materials.

RESULTS

Macrocollaterals (PcomAs, AcomA and ECA branches) in BCCAS and MCAO mice

In this study we used two inbred hypoperfusion mouse models (BCCAS and MCAO) (**FigS1 A, B**) with C57Bl/6J background to describe and analyse collateral artery plasticity in response to acute and chronic brain hypoperfusion.

We show that in naïve mice PcomAs are very small and not identifiable on MRA, basilar artery and posterior cerebral arteries, respectively affluents and effluents of PcomAs, are subtle (**Fig1 A, FigS3 A**). By contrast, in presence of an acute focal ischemia PcomAs become prominent vessels up to ≈60% of the basilar artery diameter. Their recruitment in the first hours post-surgery is essential for the mouse survival and CBF sustainment and it is characterized by an increasingly intense MRA signal (**Fig1 C, D; Fig2 A-C; FigS3 B-D**). These MRA findings have been confirmed with anatomical ones (Evans Blue and WGA CoW stainings in naïve, BCCAS and MCAO mice)(**Fig 1 A-D; Fig 3 G, M; Fig S2 A, B; Fig S3**)

Among the nodes of the collateral artery circuit (anterior communicating artery [AcomA], PcomAs, ECA, ophthalmic artery and leptomeningeal vessels and other deep microcollaterals) PcomAs display a different degree of patency, critically influencing the ischemic lesion volume, resolution and overall CBF recovery. The atresia of the PcomA ipsilateral to the MCAO and the hypoplasia of one PcomA together with the late recruitment of ipsilateral external carotid artery retrograde flow in BCCAS are likely responsible for lethal strokes affecting up to 34% of one hemisphere (12/27 [44.4%] and 3/13 [23%] mice in BCCAS and MCAO, respectively)(**Fig1 E-J**)

On the other hand, the presence of small to very prominent PcomAs (15/27 (55.5%) and 10/13 (77%) BCCAS and MCAO mice, respectively) guaranteed the survival during the most severe hypoperfusion (one day post-surgery, ≈70-80% CBF drop) (**Fig1 E-F; FigS3 B-D**).

Moreover, in a minority of mice the collateral recruitment was particularly rapid and effective, leading to no lesions (defined as white or gray matter hyperintensities) detectable on T2 MRI during the first week post-surgery (BCCAS 2/27 [7.4%], at least 1 prominent PcomA together with bilateral recruitment of ECA retrograde flow 1 day post-surgery) (**Fig2 F; TableS1**) or small lesions (1-5% of the left hemisphere) confined to striatum and dorsal part of the prefrontal cortex (MCAO, 7/13 [53.8%], prominent/very prominent left PcomA) (**Fig3 A, O**).

BCCAS (30% stenosis of both CCAs: left CCA stenosis [surgery day 1], right CCA stenosis [surgery day 2])

BCCAS is the result of a 2-day surgery beginning first with a left CCA stenosis of approximately 30% and after one day with the stenosis of the right CCA (**FigS1 A**). The compensatory mechanisms activated at day 1 deeply affect also day 2 outcome. The CBF reduction in the left hemisphere 1 day post-surgery reaches an average of 72% (20%-98%) in left striatum and frontal cortex (**Fig2 G; TableS2; TableS3**).This severe CBF drop likely instantly recruits a) left PcomA, b) AcomA and c) left ECA retrograde flow (**Fig2 A-B**). The AcomA likely redistributes blood flow from the right to the left hemisphere, with an overall reduction of right CBF and a consequent increased vulnerability for ischemic lesions during the surgery on this remaining side. Indeed, 1 day post-surgery, arterial border zones between right ACA and right MCA were the most susceptible areas (**Fig2 Ba; FigS4; FigS5**).

20/27 mice (74%) presented small to moderate ventral subcortical lesions affecting overall 1%-37% of the right hemisphere and particularly, right striatum (17/20 [85%]), prefrontal cortex (14/20 [70%]), hippocampus (10/20 [50%]), corpus callosum (5/20 [25%]) (**Fig2 H; TableS4**). These lesions were associated with a right CBF reduction which was more severe (82% [range: 60%-95%]), compared to the one observed in the left side (**Fig2 G; TableS2; TableS3**) and to the absence of retrograde flow from right ECA, which, on the contrary, was already present in the left side (**Fig2 A-B**).

Recruitment of retrograde flow from ECA and PcomA patency are the main factors influencing CBF and therefore lesion extension and overall recovery (**Fig1 F,J; Fig2; FigS5**). However, the significant intra-strain variability of PcomAs and ECA retrograde flow recruitment lead to markedly different degrees of hypoperfusion. Among the mice with at least one patent PcomA, surviving during the first week post-surgery (15/27 [55.5%]), we identified three main neuroimaging and vascular phenotypes: 1) mice presenting small subcortical lesions,

generally affecting right watershed areas (5%-20% of the right striatum and corpus callosum, 10/15 [66.6%]), displaying at least one prominent and one small PcomAs and retrograde flow from left ECA at day 1(**Fig2 A-C, D; FigS5 A; TableS1**); 2) mice presenting different degrees of ischemic lesions in the left hemisphere (3/15 [20%]), associated to absence of retrograde flow from left ECA and 1 prominent PcomA (**Fig2 E; FigS5 B; TableS1**) and 3) mice with no ischemic lesions both at one day and 7 days post-surgery (2/15 [13.3%]), displaying at least one prominent PcomA and retrograde flow from both ECAs (**Fig2 F; FigS5 C; TableS1**). Importantly, even if the CBF drop may not cause ischemic lesions detectable on T2 MRI, mild hypoperfusion leads to migration and activation of microglia/macrophages and astrocytes (**FigS6**).

External-internal carotid shunt via ophthalmic artery in BCCAS mice

Although we could not assess the ophthalmic artery flow using a Doppler, we have used angiography and histology to study the retina. Seven days post-surgery, we report severe retina degeneration with gliosis particularly in the ganglion cell layer and moderate loss of presynaptic protein CTBP2 in the outer plexiform layer. During chronic hypoperfusion we observe severe thinning and retinal atrophy mostly in the ganglion cell layer and inner nuclear layer, with significant reduction of CTBP2 signal (**FigS7 A-C**)**.** Despite the recruitment of ancillary branches of the ECA and a likely external-internal shunt, as already reported in patients with internal carotid occlusive disease [10,11], we show that retinal degeneration is irreversible and this is likely due to either the late recruitment of retrograde flow through the ECA or the pre-existence of external-internal carotid shunt (retrograde flow from the eye to the brain) via ophthalmic artery or both with an overall reduction of blood flow to the retina.

MCAO (Left MCA, CCA and ECA occlusion)

MCAO is the result of surgery consisting in the 60 minute transient blockage of left MCA and permanent occlusion of CCA and ECA (all in one session) (**FigS1 B**). This causes a significant drop in CBF in the ipsilateral hemisphere. One day post-surgery the average CBF reduction is ≈60% (range: 22%- 81%) in ipsilateral striatum and frontal cortex (**TableS5, S6**). This acute and severe hypoperfusion, likely causes a hemodynamic gradient between anterior hypoperfused brain areas and posterior areas normally perfused. The blood flow in left PcomA and the more

intense AcomA signal, detected 1 day post-surgery on MRA, is an indirect indication of left PcomA and AcomA patency (**Fig3 C-F and K, L**). A new global and stable hemodynamic balance close to the baseline is reached in 9/10 (90%) mice seven days post-surgery (**Table S5**) and left PcomA and AcomA from ancillary vessels became critical vessels (**Fig3D-G, K-L; FigS8 A**).

Despite this general pattern, high intra-strain variability of PcomA patency is the most important factor in determining the stroke outcome. Indeed, it significantly influences the lesion volume, the lesion extension, the CBF recovery and the contralateral drop in CBF (**Fig3 O-R; Table S6, S7**). In our cohort we report a spectrum of left PcomA sizes, from non-patent and small (**Fig3 M**, 4/13 (30.7%) and 2/13 (15.4%), respectively) to promiment and very prominent (**Fig3 G**, 6/13 (46%) and 1/13 (7.7%), respectively). Mice with left non-patent PcomA died within few hours post-surgery. MCAO mice with a small left PcomA (**Fig3 M; S8 B**) displayed the largest lesions affecting up to 34% of the left hemisphere (**Fig3 B**) and including also dorsal areas (orbital cortex and cerebellum) (**Fig3 B, O, P; Table S8**), the most severe drop in CBF (up to 80% in left striatum) (**Fig3 Q, R**), the slowest recovery (up to 4 weeks) (**TableS5**) and a marked brain atrophy (**Fig3 N**). In these mice, we observed a significant proportional compensatory decrease of contralateral CBF (up to 30% in right striatum, **Fig3 Q**). In comparison, mice with prominent left PcomA (**FigS8 A**) showed lesions 2.6 times smaller (**Fig3P; TableS7**), mostly affecting ventral areas (prefrontal cortex, striatum and ventral hippocampus) (**Fig3 O**) and a moderate drop in ipsilateral and contralateral CBF (≈57% and 15% in left and right striatum, respectively) (**Fig3 Q**). Very prominent PcomA (**Fig3 G**) was associated to the smallest lesions (5% of the left hemisphere) (**Fig3 A**), mild CBF reduction and more rapid recovery (**Fig3 Q, R**) and absence of macroscopic ipsilateral brain atrophy (**Fig3 H**)

In the supplementary we describe in details the extreme phenotypes. The other cases fall within this phenotypic spectrum (**FigS8**)

The hemisphere contralateral to MCAO

In MCAO mice, the blood flow redistribution from the right to the left hemisphere via AcomA causes a significant and proportional CBF reduction in the right hemisphere: 17% (range: 4%-33%), 28% (range:18-41%) in striatum and frontal cortex, respectively (**Fig3 Q; TableS5, S6**). Interestingly, MCAO mice with small left PcomA display significantly lower global CBF values, both for the left and right hemisphere at day one (**Fig3 Q**; **TableS5, S6**) and right CBF reduction

(≈30% in right striatum) which is close to the CBF reduction seen in BCCAS mice with the most effective vascular phenotype (retrograde flow from both ECAs and 2 prominent PcomAs) (≈40%) at day 7 (**TableS6, S3**). This pattern mimics the hemodynamic effects of unilateral CCA stenosis and therefore triggers analogous compensatory mechanisms such as right ECA retrograde flow, although temporarily and only during the first 24 hours post-surgery (**FigS8 C**)**.** On the contrary, a more stable involvement of the contralateral hemisphere is evident at the microvascular level (leptomeningeal arterioles and deep microvessels), where increased number of larger arterioles and a more dense vascular network is detected in the infarct and peri-infarct areas, respectively, 7 weeks post-surgery (**Fig4, 5, 6**).

Microcollaterals (leptomeningeal and deep arterioles) in BCCAS and MCAO mice

In both models part of the microvessels likely represent microcollaterals, given the increased number of vessel length, vascular junctions and reduction of end points compared to naïve mice (**Fig5E-G**). These microvessels display in the cortical and deep gray matter a similar pattern whereas white matter arterioles appear significantly rare and sparse (**Fig4, 5; FigS9; FigS10**)

Infarct and peri-infarct areas and other hypoxic regions are characterized by significantly different microvascular features. Increased size up to 50μm diameter and reduced density of arterioles are a hallmark in the infarct area(**Fig4 A-CIV; TableS9**). Their increased diameter is associated with a significant invasion of microglia/macrophages, generally in the form of islets (**Fig4 CI, CII**) during the hypoxic subacute phase whereas activated astrocytes are detected in the peri-infarct area and delimit the infarct-peri-infarct border (**Fig4 CIII)**. By contrast, the peri-infarct area and moderately hypoperfused regions are characterized by a network of microvessels with moderately increased length and whose number of anastomoses is proportional to the degree of hypoperfusion (highest density of junctions in right and left hemisphere in BCCAS and MCAO mice, respectively)(**Fig5 E; Table S10**).Importantly, in MCAO this phenomenon affects also the relatively hypoperfused hemisphere contralateral to the focal ischemia and at the leptomeningeal superficial level gives rise to a symmetric picture, with both right and left leptomeningeal vessels presenting overlapping vascular anastomoses, vessel density and length 7 weeks post-surgery(**Fig6 C-F; TableS11**).

DISCUSSION

The aim of the study was to capture the collateral vessel evolution during brain ischemia and to comprehensively describe the hemodynamic changes over time (2 days, 7 days, 4 and 7 weeks) in 2 widely used experimental models of brain hypoperfusion with C57/BL6 J background: MCAO and BCCAS.

We show that contralateral hemisphere, vertebrobasilar circulation and retrograde flow from ECA represent 3 essential reservoirs for the CBF redistribution during focal ischemia. In presence of acute ischemia, these 3 pools, normally independent, are interconnected by AcomA, PcomAs and ECA ancillary branches and become a pivotal and integrant part of the same hemodynamic circuit. Moreover, the partial functional overlap between them leaves the possibility for some backup solutions.

PcomAs are the main determinants of stroke survival in MCAO. First, MCAO mice with no/non-patent PcomAs die within 24 hours post-surgery. Second, MCAO mice display lesion volume, lesion resolution and ipsi and contralateral CBF reduction proportional to the left PcomA calibre, with mice with small and very prominent PcomAs showing the biggest and smallest lesion volumes and least and most effective lesion resolution, respectively(**Fig3**). Analogously, PcomA patency together with the promptness of ECA retrograde flow recruitment play a key role in BCCAS.

Overall, in both these hypoperfusion mouse models we report a similar percentage of PcomA variability with 15.4% and 37% mice with none or 2 non-patent PcomAs, 30.8% and 22.2% mice with at least 1 small PcomA, 53.8% and 37% with one prominent/very prominent PcomA and 33.3% mice with 2 prominent PcomAs. By contrast, McColl et al reported in the same C57BL/6 strain 3/10 (30%), 6/10 (60%) and 1/10 (10%) mice with none, one and 2 PcomAs, respectively [3].This difference may be due to 3 main factors: first, McColl studied the collateral status in naïve mice and we show that collaterals are recruited under moderate-severe acute hypoxia, therefore representing a functional vascular phenotype that can only be seen in response to ischemia. Thus, the presence of very subtle vessels in naïve mice does not imply their potential patency. Second, the small sample size that can significantly bias the results. Third, PcomAs size represents a dynamic spectrum, varying significantly from non-patent to very prominent and therefore an unambiguous classification is difficult to draw.

A growing body of evidence reported hemodynamic, metabolic, neuroimaging and functional changes in the stroke contralateral hemisphere in the acute phase (first hours-days post ischemia) [12,13,14,15,16]. Here, we provide evidence that the contralateral hemisphere represents an important reserve of blood flow that can be shifted to the ischemic focus, to counterbalance any CBF gradient. First, the average reduction of right CBF in the BCCAS model (≈83%) is higher compared to the hypoperfusion detected in left hemisphere (≈72%), likely due to the pre-existent right to left CBF shunt due to the surgery on left CCA at day 1, the left-right CBF gradient drop and the later recruitment of the right ECA. Consequently, the right ACA territory and the border zones between right MCA and right ACA become particularly susceptible to ischemic lesions (**Fig2 Ba; FigS4 and S5**). Second, MCAO right CBF reduction is proportional to the reduction of CBF in the left hemisphere and thus to the left PcomA calibre (**Fig3 Q; TableS6**). This is in line with previous studies in patients that measured CBF with positron emission tomography (PET) and found a significant correlation between flow impairment in the ischemic area and proportional CBF reduction in the contralateral hemisphere [12]. Third, the CBF drop in MCAO mice with small left PcomA(up to 37% of the pre-surgery value) is very close to the CBF reduction seen in BCCAS mice with two prominent PcomAs and retrograde flow from both ECAs 7 days post-surgery (≈ 40%) (**TableS3, S6**). Therefore, this simulates the hemodynamic effects of a CCA stenosis and thus temporarily triggers the same compensatory mechanisms such as right ECA retrograde flow (**FigS8 C**). Moreover, the critical importance of the contralateral hemisphere in the sustainment of the CBF is highlighted by the different time of recovery between MCAO mice and BCCAS. 90% of MCAO mice recover almost to the baseline after one week whereas BCCAS mice take 4 weeks [7]. Finally, the significant involvement of the contralateral hemisphere leads to a moderate hypoperfusion that even if it is not sufficient to cause ischemic lesions and remains below the threshold of T2 weighted MRI detectability, is responsible for a significant microvascular remodelling at different levels: from the superficial leptomeningeal to the deep striatal layers (**Fig5; Fig6**).

Analogously to the peri-infarct area, moderately hypoxic ipsilateral and contralateral areas are covered with a dense network of microvessels with moderately increased length and significantly augmented anastomoses (**Fig5**). Given its hemodynamic features, this microvascular phenotype likely results in a greater perfusion volume thus improving the tissue oxygenation and the uptake of catabolites. Moreover, this vascular web likely exerts a

trophic function through the synthesis and release of neurotrophins such as NGF, IGF-I, and BDNF, that further catalyse the long-lasting vessel formation and recruitment of immune cells [17]. Therefore, this hypoxia-triggered-vascular plasticity may shape and significantly influence pre-existent neuronal circuits, explaining neurophysiologic changes also in the contralateral hemisphere [18].

By contrast, and as already reported in stroke patients [19], the infarct area is characterized by rarefied arterioles with increased diameter, up to 4.5 times the diameter of the largest arterioles observed in the respective brain regions in naïve mice (**Fig4; TableS9**). These vascular features assure a reduced resistance and are particularly effective for a rapid delivery of microglia/macrophages, removing debris and exerting a neuroprotective function in the subacute phases (7 days post-surgery) (**Fig4 CI, CII**) [20,21].

In addition, the abrupt redistribution of blood in ancillary vessels or vessel normally characterized by lower intravascular pressure causes macromodifications such as increased tortuosity, which is a hallmark of intravascular hypertension (**Fig3M, blue arrow; FigS8 A,B**) [22,23]. Over time, this may lead to 1) arteriolar ialinosis in microvessels [24], with an increased risk for subcortical microbleeds, already reported in the same BCCAS model, 6 months post-surgery [7] and differing from amyloid related microbleeds, given the main subcortical location and the absence of lobar involvement [25] and 2) aneurisms in macrovessels [22,23]. Therefore, strengthening a possible cause-effect link between ischemic and haemorrhagic strokes, supported already by several genetic risk factors such as *COL4A1* associated to both [26,27].

Finally, we showed that the BCCAS model, which has been used as an experimental model of chronic hypoperfusion is firstly characterized by an acute and severe hypoperfusion leading to the rapid vascular response and ischemic lesions particularly affecting subcortical and watershed areas (striatum, corpus callosum and prefrontal cortex). The acute hemodynamic compensatory response leads to a gradual recovery and in the long-term a modest hypoperfusion. Therefore, BCCAS mice significantly differ from patients, where chronic hypoperfusion is a gradual phenomenon, occurring in years or decades and leaving the time for a progressive adaptation of collateral circulation both at the level of the circle of Willis and leptomeningeal collaterals. The compensatory responses triggered during this acute and most severly hypoperfused phase (1 day) are the main determinants of the long-term outcome both in terms of lesion volume, extension, recovery and brain atrophy. Thus, the loss of neurons reported in corpus callosum in the chronic phase in this BCCAS model [28] may be

attributable to ischemic lesions and acute severe drop in CBF, rather than resulting from chronic mild global hypoperfusion.

In summary, we show that focal ischemia triggers a global hemodynamic response, significantly affecting also the contralateral hemisphere until the effective re-establishment of a new hemodynamic balance. Acute hypoperfusion immediately leads to a negative selection of mice with no PcomAs. PcomA patency ipsilateral to the focal ischemia decides the infarct volume and recovery in MCAO mice. Similarly, the rapidity of retrograde ECA blood flow recruitment, together with PcomA patency, mainly shape the extension and the side of ischemic lesions in BCCAS mice. Finally, given the significant intrastrain collateral variability, when using C57/BL6J mice as MCAO and BCCAS ischemia models to test the independent effect of neuroprotectants and genes on stroke outcome, PcomAs and the overall collateral recruitment particularly during the most severe brain hypoperfusion (1-7 days post-surgery) have to be critically considered as additive and main factors influencing brain lesions and perfusion recovery.

Acknowledgements

NeuroCure, Deutsches Zentrum für Neurodegenerative Erkrankungen (DZNE), Alexander von Humboldt Fellowship (to Celeste Sassi).

Author Contribution statement

C.S, M.F,K.W and U.D and planned the experiments. C.S, M.F and K.W performed the experiments. C.S, M.F,K.W, U.D, K.B, S.M, S.B, N.R, S.CG, D.H, A.I, A.M, A.J, O.S, D.B took part to the result analysis and manuscript revision

Disclosure/Conflict of Interest

We do not report any conflict of interest.

References

1. Shuaib A, Butcher K, Mohammad AA, et al. Collateral blood vessels in acute ischaemic stroke: a potential therapeutic target. *Lancet Neurol* 2011; 10: 909–921.

2. Faber JE, Moore SM, Lucitti JL, et al. Sex Differences in the Cerebral Collateral Circulation. *Transl Stroke Res* 2017; 8: 273–283.

3. McColl BW, Carswell HV, McCulloch J, et al. Extension of cerebral hypoperfusion and ischaemic pathology beyond MCA territory after intraluminal filament occlusion in C57Bl/6J mice. *Brain Res* 2004; 997: 15–23.

4. Wang S, Zhang H, Dai X, et al. Genetic architecture underlying variation in extent and remodeling of the collateral circulation. *Circ Res* 2010; 107: 558–568.

5. Chalothorn D, Clayton JA, Zhang H, et al. Collateral density, remodeling, and VEGF-A expression differ widely between mouse strains. *Physiol Genomics* 2007; 30: 179–191.

6. Lucitti JL, Sealock R, Buckley BK, et al. Variants of Rab GTPase-Effector Binding Protein-2 Cause Variation in the Collateral Circulation and Severity of Stroke. *Stroke* 2016; 47: 3022–3031.

7. Boehm-Sturm P, Füchtemeier M, Foddis M, et al. Neuroimaging Biomarkers Predict Brain Structural Connectivity Change in a Mouse Model of Vascular Cognitive Impairment. *Stroke* 2017; 48: 468–475.

8. Martin NA, Bonner H, Elkjær ML, D'Orsi B, Chen G, König HG, et al. BID Mediates Oxygen-Glucose Deprivation-Induced Neuronal Injury in Organotypic Hippocampal Slice Cultures and Modulates Tissue Inflammation in a Transient Focal Cerebral Ischemia Model without Changing Lesion Volume. Front Cell Neurosci. 2016;10:14.

9. Zudaire E, Gambardella L, Kurcz C, et al. A computational tool for quantitative analysis of vascular networks. *PLoS ONE* 2011; 6: e27385.

10. Kerty E, Nyberg-Hansen R, Hørven I, et al. Doppler study of the ophthalmic artery in patients with carotid occlusive disease. *Acta Neurol Scand* 1995; 92: 173–177.

11. Kerty E, Eide N, Hørven I. Ocular hemodynamic changes in patients with high-grade carotid occlusive disease and development of chronic ocular ischaemia. II. Clinical findings. *Acta Ophthalmol Scand* 1995; 73: 72–76.

12. Lagrèze HL, Levine RL, Pedula KL, et al. Contralateral flow reduction in unilateral stroke: evidence for transhemispheric diaschisis. *Stroke* 1987; 18: 882–886.

13. Lavy S, Melamed E, Portnoy Z. The effect of cerebral infarction on the regional cerebral blood flow of the contralateral hemisphere. *Stroke* 1975; 6: 160–163.

14. Takatsuru Y, Eto K, Kaneko R, et al. Critical role of the astrocyte for functional remodeling in contralateral hemisphere of somatosensory cortex after stroke. *J Neurosci* 2013; 33: 4683–4692.

15. Krakauer JW, Radoeva PD, Zarahn E, et al. Hypoperfusion without stroke alters motor activation in the opposite hemisphere. *Ann Neurol* 2004; 56: 796–802.

16. Sbarbati A, Reggiani A, Nicolato E, et al. Regional changes in the contralateral 'healthy' hemisphere after ischemic lesions evaluated by quantitative T2 parametric maps. *Anat Rec* 2002; 266: 118–122.

17. Carmeliet P. Blood vessels and nerves: common signals, pathways and diseases. *Nat Rev Genet* 2003; 4: 710–720.

18. Baron JC, Rougemont D, Soussaline F, et al. Local interrelationships of cerebral oxygen consumption and glucose utilization in normal subjects and in ischemic stroke patients: a positron tomography study. *J Cereb Blood Flow Metab* 1984; 4: 140–149.

19. Xu C, Schmidt WUH, Galinovic I, et al. The potential of microvessel density in prediction of infarct growth: a two-month experimental study in vessel size imaging. *Cerebrovasc Dis* 2012; 33: 303–309.

20. Kawabori M, Kacimi R, Kauppinen T, et al. Triggering receptor expressed on myeloid cells 2 (TREM2) deficiency attenuates phagocytic activities of microglia and exacerbates ischemic damage in experimental stroke. *J Neurosci* 2015; 35: 3384–3396.

21. Jin W-N, Shi SX-Y, Li Z, et al. Depletion of microglia exacerbates postischemic inflammation and brain injury. *J Cereb Blood Flow Metab* 2017; 37: 2224–2236.

22. Shimada K, Furukawa H, Wada K, et al. Protective Role of Peroxisome Proliferator-Activated Receptor-γ in the Development of Intracranial Aneurysm Rupture. *Stroke* 2015; 46: 1664–1672.

23. Silva RAP, Kung DK, Mitchell IJ, et al. Angiotensin 1–7 Reduces Mortality and Rupture of Intracranial Aneurysms in MiceNovelty and Significance. *Hypertension* 2014; 64: 362–368.

24. Wiener J, Spiro D, Lattes RG. THE CELLULAR PATHOLOGY OF EXPERIMENTAL HYPERTENSION. II. ARTERIOLAR HYALINOSIS AND FIBRINOID CHANGE. *Am J Pathol* 1965; 47: 457–485.

25. Greenberg SM, Vernooij MW, Cordonnier C, et al. Cerebral microbleeds: a guide to detection and interpretation. *Lancet Neurol* 2009; 8: 165–174.

26. Gould DB, Phalan FC, van Mil SE, et al. Role of COL4A1 in small-vessel disease and hemorrhagic stroke. *N Engl J Med* 2006; 354: 1489–1496.

27. Weng Y-C, Sonni A, Labelle-Dumais C, et al. COL4A1 mutations in patients with sporadic late-onset intracerebral hemorrhage. *Ann Neurol* 2012; 71: 470–477.

28. Shibata M, Ohtani R, Ihara M, et al. White matter lesions and glial activation in a novel mouse model of chronic cerebral hypoperfusion. *Stroke* 2004; 35: 2598–2603.

LEGENDS

Fig1

PcomA and vascular phenotype effect in MCAO and BCCAS mouse models. A-D. PcomA calibre in normal and ischemic conditions. **A**. Non-patent right PcomA (**2a**), detected in a naïve mouse; **B** non-patent right PcomA (**2a**) and absence of left PcomA (**2b**) in MCAO sham; **C** prominent left PcomA (**2b**) and non-patent right PcomA (**2a**) in MCAO; **D** 2 prominent PcomAs in BCCAS (**2a, 2b**). 1, basilar artery (BA); 2a, right PcomA; 2b, left PcomA; 3a, right posterior cerebral artery (PCA); 3b, left posterior cerebral artery (PCA). The numbering of the vessels reflects the direction of the collateral blood flow following focal ischemia in the MCA or anterior brain areas: BA→PcomA→PCA, as already described in detail in the BCCAS and MCAO models in **Fig S1 A** and **B. E-F** Effect of left PcomA size and PcomA-ECA retrograde flow in MCAO and BCCAS survival. MCAO mice with non-patent left PcomA die few hours post-surgery. ≈ One-fourth of mice with small left PcomA die within one day post-surgery. The majority of MCAO mice with small left PcomA and all the MCAO with prominent/very prominent PcomA survive (**E**). Analogously, BCCAS mice with no PcomAs or no PcomA-no ipsilateral ECA retrograde flow die within few hours post-surgery. By contrast, BCCAS mice with at least one small to prominent PcomA and retrograde flow from left or right ECA do survive. **G-H** MCAO mice with non-patent left PcomA died within 1 day post-surgery with ischemic lesions affecting more than 35% of the left hemisphere and left PcomA and overall left blood flow were not identifiable on MRA one day post-surgery. **I-J**. BCCAS with non-patent right PcomA (*) and absence of right ECA retrograde flow recruitment (**), presenting severe ischemic lesions affecting >20% of the right hemisphere.

Fig2

MRA and MRI phenotypes in BCCAS mice 1-7 days post-surgery. **A-C.** Vascular collateral plasticity during the first week post-surgery; **a**, circle of Willis; **b**, ECA flow **A.** Pre-surgery MRA, where PcomAs are not identifiable. **B** MRA 1d post-surgery, showing recruitment of both PcomAs (white arrows), directing the blood flow to the PCAs, whose MRA intensity is increased, and left ECA retrograde flow (green arrow, yellow dashed line) and hypoperfused border zones between right ACA and right MCA (a, orange arrow). **C**. MRA 7d post-surgery, characterized by increased PcomA (white arrows) and PCAs MRA intensity signal, recruitment of right ECA retrograde flow (green arrow, yellow dashed line), with a compensatory sustainment of the right anterior cerebral artery (ACA) territory (a, orange arrow) partially coming from the left hemisphere through the AcomA (blue dashed line). **D-F**. Main ischemic lesion patterns observed in BCCAS 24h post-surgery on T2-weighted MRI: small right subcortical lesions (**D**), big cortical and subcortical lesions (**E**) and no lesions detectable (**F**). **G**. Percentage of CBF reduction at day 1 in BCCAS mice in left and right hemispheres, displaying more accentuated hypoperfusion in the right hemisphere, particularly in the frontal cortex. **H**. Most affected brain regions in the BCCAS model 1 day post surgery are the watershed areas between right ACA and right MCA: right cerebral cortex, corpus callosum, striatum und

hippocampus. CCA L, left common carotid artery; ECA L, left external carotid artery; ECA R, right external carotid artery; PCA L, left posterior cerebral artery; PCA R, right posterior cerebral artery; PcomA L, left posterior communicating artery; PcomA R, right posterior communicating artery. R, right; L, left. Pre-Op, pre-surgery.

Fig3

Effect of PcomA in MCAO. **A-B**, ischemic lesions (red shades) identified on T2-weighted MRI. **A-N** Edges of the phenotypic spectrum observed in MCAO mice: small lesion (**A**) associated to very prominent left PcomA (**C-G**) and absence of macroscopic left atrophy (**H**). **C-D,** recruitment of left PcomA is identifiable on MRA 1 day post-surgery (white arrow) and it is accompanied by increased intensity of left PCA (blue arrow)**. B,** Extensive lesion caused by small left PcomA (**I-M**), leading to significant left brain atrophy (**N**). E-F and K-L progressive increase in the AcomA size (yellow arrows). **O-R** PcomA size is the most important factor in determining lesion volume during acute hypoperfusion (1d), infarct resolution during subacute hypoperfusion (7d) (**O**, **P, Q**), ipsilateral and compensatory contralateral CBF decay in ventral ischemic regions such as striatum (**Q, R**). Detailed description of MCAO mice phenotype as well as collateral blood flow direction are provided in the supplementary materials. Small, prominent and very prominent refer to the left PcomA size. SL, striatum left; SR, striatum right; d, day/s; w, weeks.

Fig4

Microvascular plasticity in the infarct area in MCAO and BCCAS models. The infarct area is characterized by arterioles reduced in number and increased in size both at the leptomeningeal level (**A**) and striatal one (**B-CIV**)(**white arrows**), generally associated in the subacute phase (7d) to significant microglia infiltration (**CI-CII**). Scale bars: B, CI, CIII, CIV = 1mm; B', CII = 0.5mm. Mice perfused with WGA Alexa Fluor® 680 conjugate (Termofisher, W32465).D, day/s; wk, weeks.

Fig5

Moderately hypoperfused areas are characterized by microvessels with moderately increased length in MCAO compared to naïve mice (**A-D', F**), whose significantly increased number of anastomoses (**E-G**) is proportional to the degree of hypoperfusion at day 1(**H**). A-B' and C-D'. Microvessels stained with WGA in left and right striatum in naïve and MCAO mice, respectively. A'-B' and C'-D', angiotool analysis of the homologous histological sections (A-B and C-D). Mice perfused with WGA. Scale bars = 0.5mm. Alexa Fluor® 680 conjugate (Termofisher, W32465). L, left; R, right; CL, cortex left; CR, cortex right; SL, striatum left; SR, striatum right.

Fig6

A-F. **Leptomeningeal vessels in MCAO mice 7 weeks post-surgery**. Leptomeningeal vessels in naïve mouse (**A**) and MCAO (**B**). **C**. Anastomoses between terminal branches of PCA and

MCA in the right cortex of MCAO mice. MCAO mice are characterized by a symmetric network of leptomeningeal arterioles with increased anastomoses (**D**), density (**E**) and moderately increased vessel length (**F**), both in cortex ipsilateral and contralateral to MCAO. MCA, middle cerebral artery; PCA, posterior cerebral artery; L, left; R, right; wks, weeks.

Figures

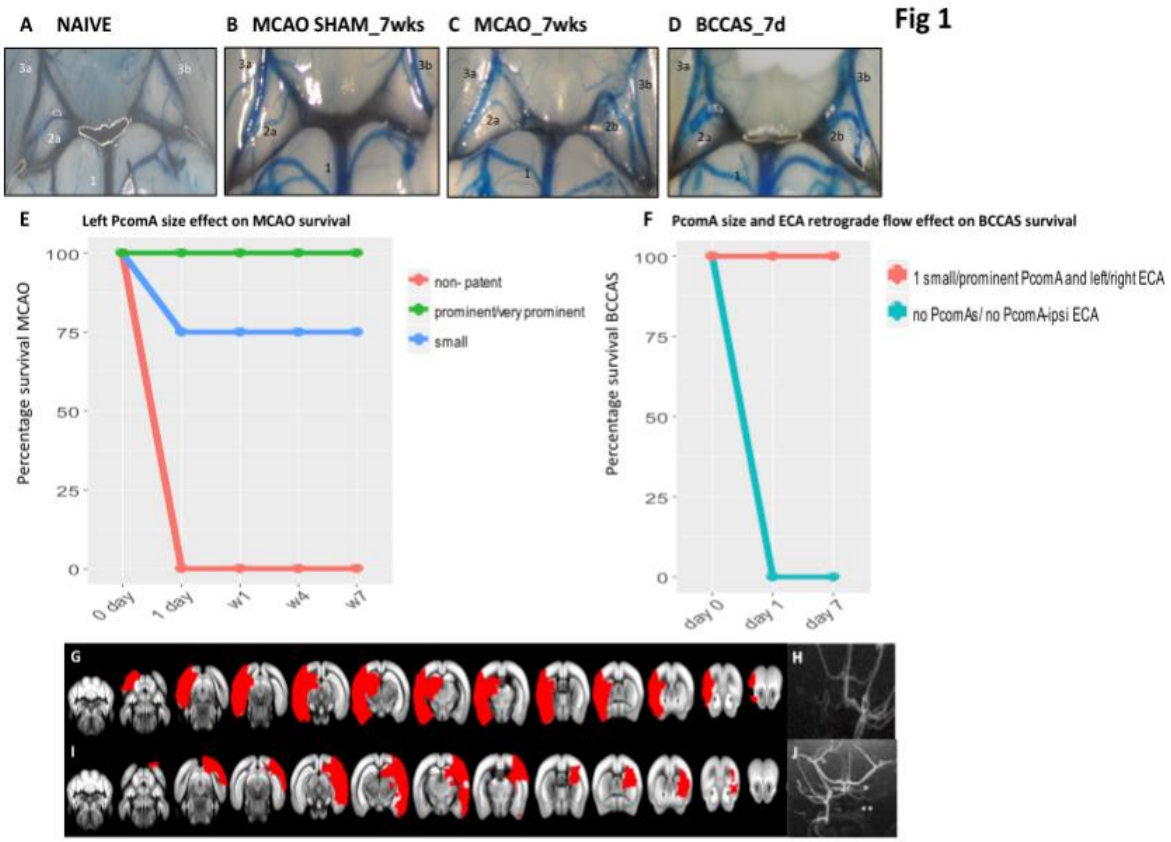

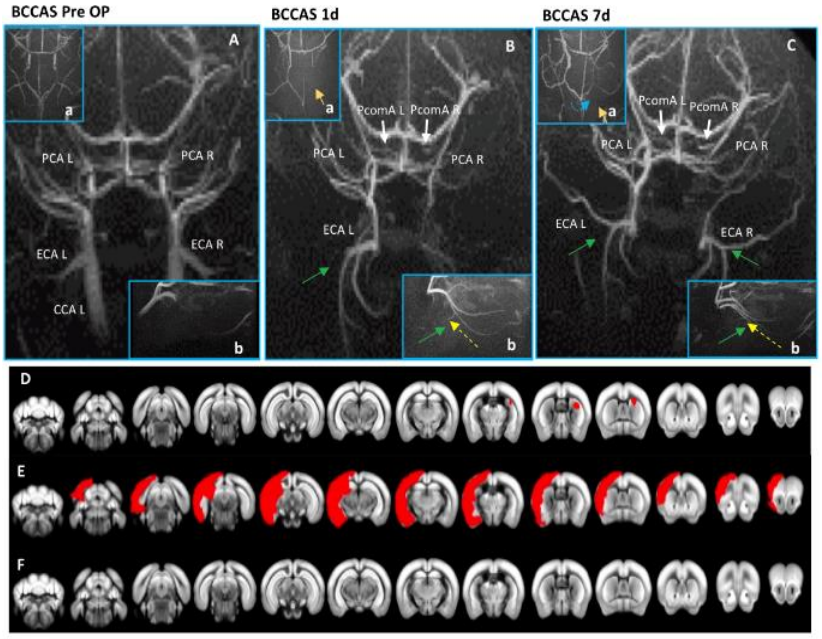
BCCAS Pre OP
BCCAS 1d
BCCAS 7d
A
B
C
a
b
PCA L
PCA R
ECA L
ECA R
CCA L
PcomA L
PcomA R
D
E
F

Fig 2

Fig 3

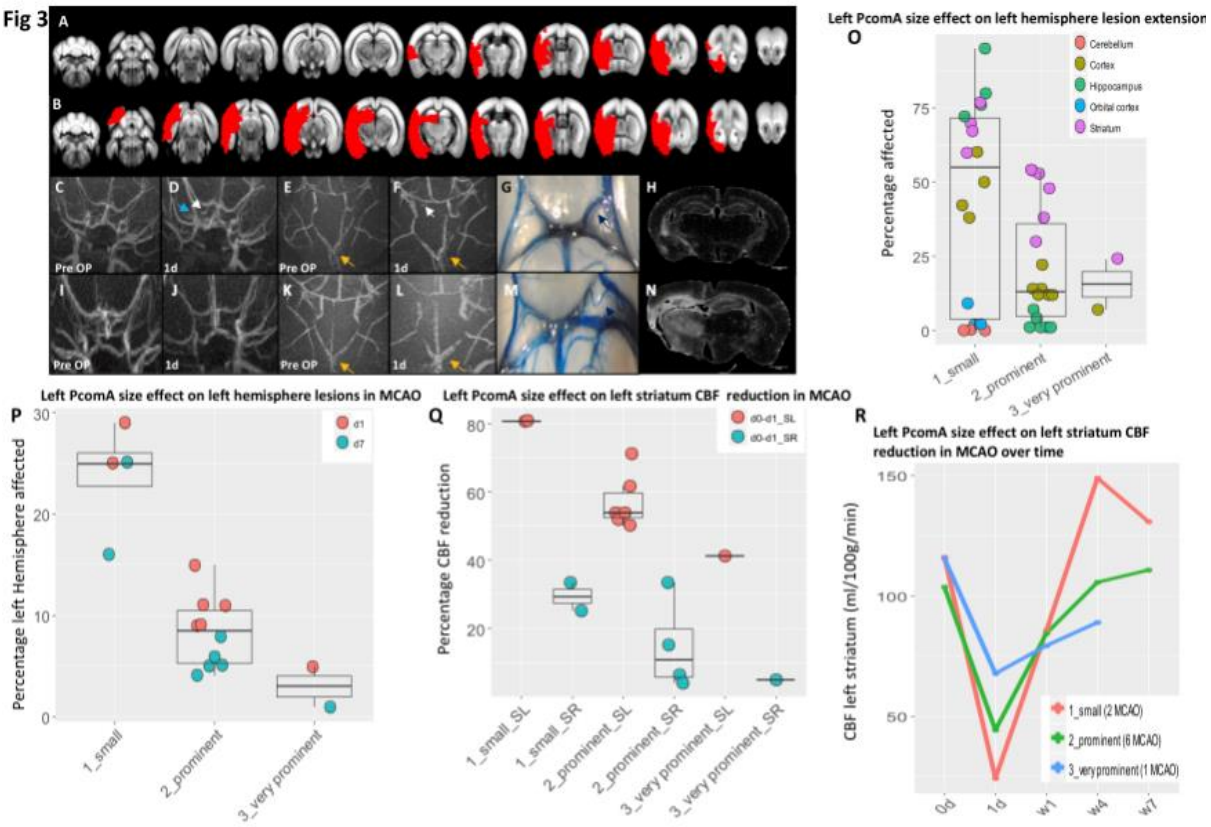
A
B
C
D
E
F
G
H
I
J
K
L
M
N
Pre OP
1d
Left PcomA size effect on left hemisphere lesion extension
O
Cerebellum
Cortex
Hippocampus
Orbital cortex
Striatum
Percentage affected
1_small
2_prominent
3_very prominent
Left PcomA size effect on left hemisphere lesions in MCAO
P
d1
d7
Percentage left Hemisphere affected
Left PcomA size effect on left striatum CBF reduction in MCAO
Q
d0-d1_SL
d0-d1_SR
Percentage CBF reduction
1_small_SL
1_small_SR
2_prominent_SL
2_prominent_SR
3_very prominent_SL
3_very prominent_SR
R
Left PcomA size effect on left striatum CBF reduction in MCAO over time
CBF left striatum (ml/100g/min)
1_small (2 MCAO)
2_prominent (6 MCAO)
3_very prominent (1 MCAO)
0d
1d
w1
w4
w7

Fig 4

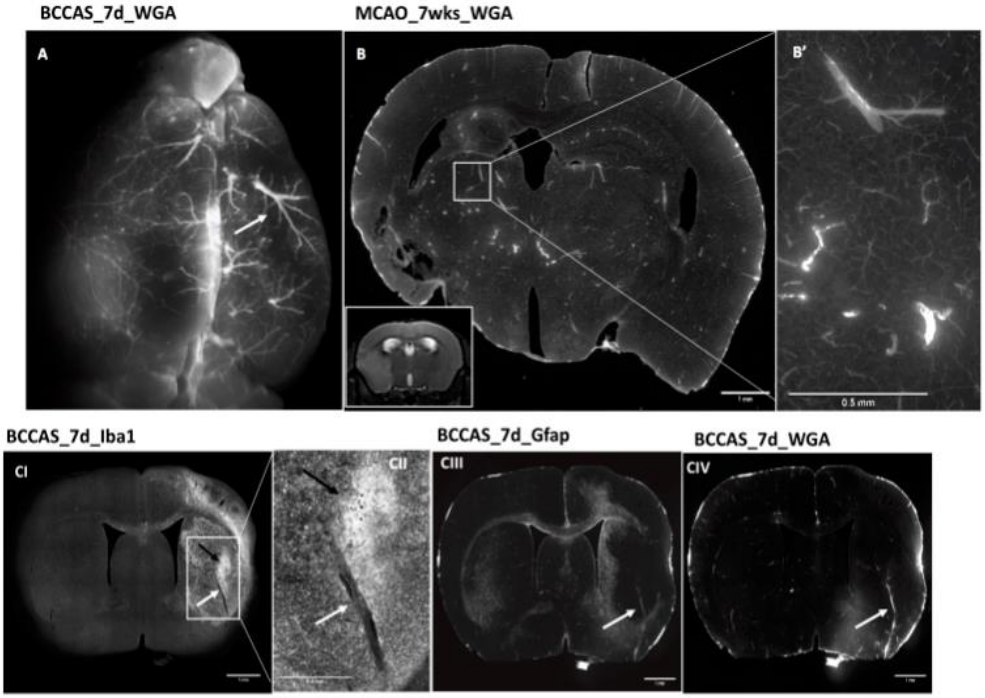
BCCAS_7d_WGA
MCAO_7wks_WGA
A
B
B'
0.5 mm
BCCAS_7d_Iba1
BCCAS_7d_Gfap
BCCAS_7d_WGA
CI
CII
CIII
CIV

Fig 5

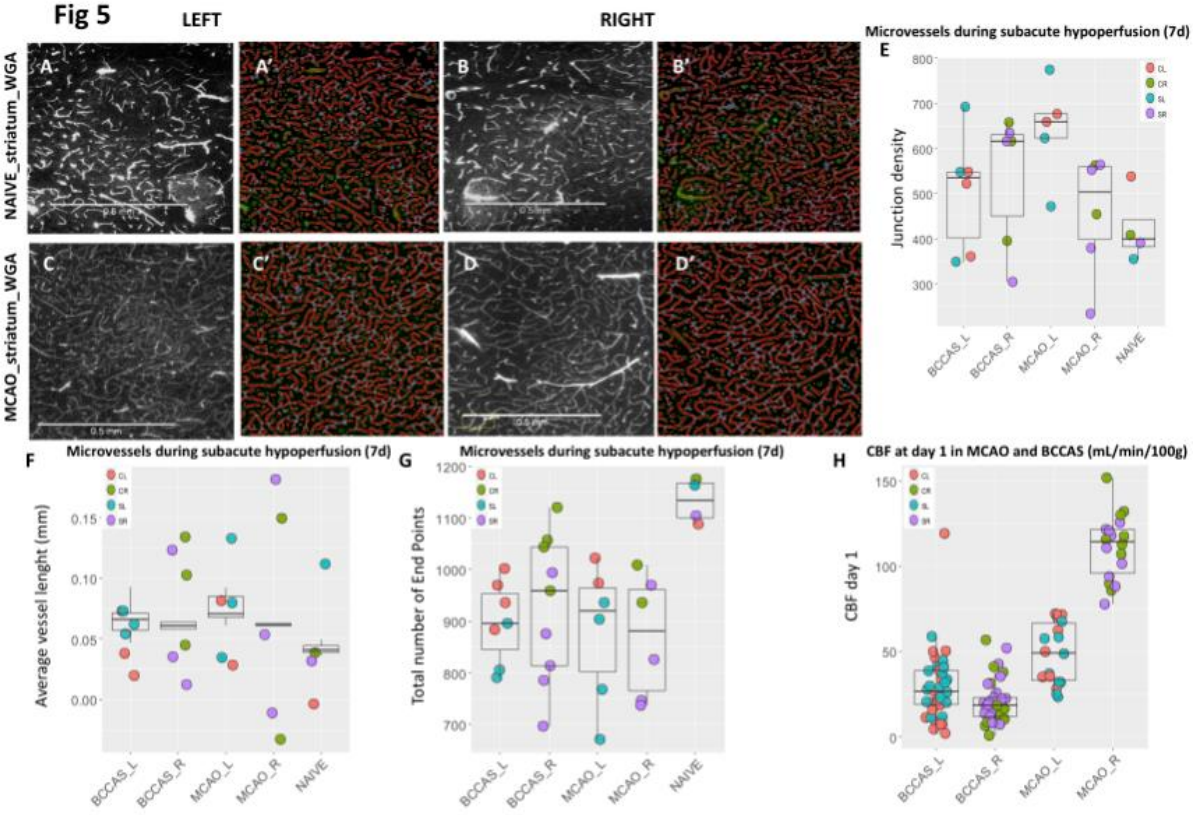
LEFT
RIGHT
NAIVE_striatum_WGA
MCAO_striatum_WGA
A
A'
B
B'
C
C'
D
D'
0.5 mm
Microvessels during subacute hypoperfusion (7d)
E
Junction density
BCCAS_L
BCCAS_R
MCAO_L
MCAO_R
NAIVE
F
Average vessel lenght (mm)
G
Total number of End Points
H
CBF at day 1 in MCAO and BCCAS (mL/min/100g)
CBF day 1

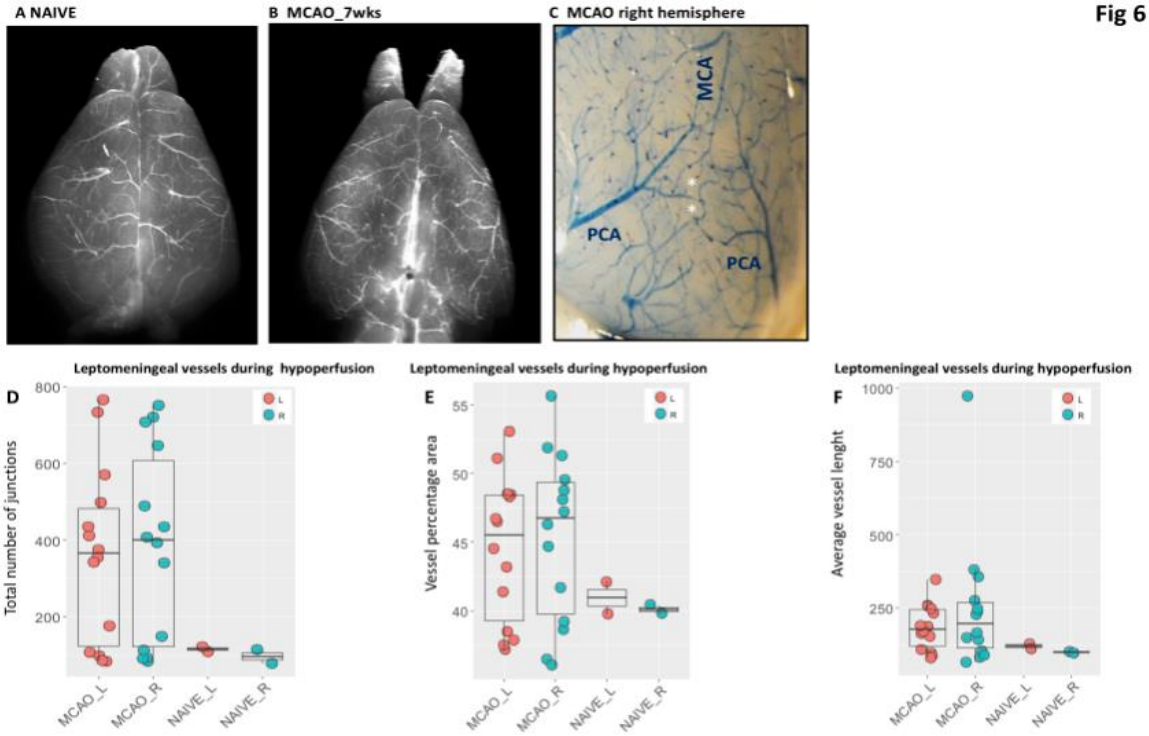

Fig 6

SUPPLEMENTARY MATERIALS AND METHODS

BCCAS

Anaesthesia was achieved using isoflurane in a 70:30 nitrous oxide:oxygen mixture and core body temperature was maintained at 37 ± 0.2 °C with an automated rectal probe and heat blanket. A midline incision was made in the neck, and a carotid artery was carefully exposed. Hypoperfusion was induced by winding a custom ordered, non-magnetic, surgical grade microcoil (160 µm inner diameter, Shannon Coiled Springs Microcoil, Limerick, Ireland) around one of the carotid arteries. The muscle and glands were guided back into place and local anaesthetic was applied to the sutured wound prior to recovery. Twenty- four hours later, the same procedure was repeated on the other carotid artery. This delay represents an important refinement that does not result in higher mortality when using the smaller sized microcoils. Regular diet was placed on the floor of the cage to assist with feeding. In the BCCAS model, hypoperfusion was induced by winding a custom ordered, nonmagnetic, surgical grade microcoil (160 µm inner diameter; Shannon Coiled Springs Microcoil, Limerick, Ireland) around one of the common carotid arteries. The muscles and glands were guided back into place, and local anesthetic was applied to the sutured wound before recovery. Twenty-four hours later, the same

procedure was repeated on the other common carotid artery. This delay represents an important refinement that does not result in higher mortality when using the smaller sized microcoils.

MCAO

In the MCAO model, hypoperfusion was induced as described previously (http://precedings.nature.com/documents/3492/version/2). Briefly, after closing the left common carotid artery (CCA) and left external carotid artery (ECA) a microvascular clip was put on the left internal carotid artery (ICA) and a small incision was made on the CCA. A nylon filament (7019PK5Re, Doccol Corp, Redlands, California, USA) was introduced over CCA and ICA to occlude the origin of middle cerebral artery (MCA) and fixed with a suture around the ICA. After 60 minutes, the filament was removed causing immediate reperfusion. Afterwards the suture on the ICA was closed. This type of MCAO surgery results in permanent occlusion of left CCA, ECA and ICA.

MRI measurements

Anaesthesia was again achieved using isoflurane as per above, and body temperature and respiration rate were monitored with MRI compatible equipment (Small Animal Instruments, Inc., Stony Brook, NY).

Cerebral blood flow and angiographies

CBF and angiography were measured on a 7 T Pharmascan using Paravision 5.1 software (Bruker BioSpin, Ettlingen, Germany). For the CBF measurement, radio frequency transmission was achieved with a 72 mm diameter quadrature resonator actively decoupled to a mouse quadrature surface coil used for reception (Bruker BioSpin, Ettlingen, Germany). A single slice (1 mm) flow-sensitive alternating inversion recovery (FAIR) sequence with a rapid acquisition with relaxation enhancement (RARE) readout was used (repetition time (TR)/recovery time/echo spacing (ΔTE)/effective echo time (TEeff): 12 000/10 000/7.2/35.9 ms, respectively, 16 inversion times (35-1500 ms), RARE factor: 32, inversion slice thickness: 4 mm, 180° hyperbolic secant (sech80) inversion pulse (20 ms), field of view (FOV): 25.6 mm2, matrix: 128 x 64 enlarged by partial fourier transform to 128 x 128, resolution: 200 µm2, 12 min). For angiography measurements, a 20 mm diameter quadrature volume coil (RAPID Biomedical, Rimpar, Germany) was used for radio frequency transmission and reception and a 3D time of light (TOF) sequence was used (TR/TE: 15/2.5 ms, α: 20 ˚, FOV: 25 mm3, resolution: 98 x 130 x 196 µm3 zero-filled to 98 µm3, 6 min). Spectroscopy, T2 weighted and MR spectra were acquired on a 7 T

Biospec with a cryogenically cooled transmit/receive surface coil and Paravision 6.0 software (Bruker BioSpin, Ettlingen, Germany).

A 2D RARE T2 sequence was used for anatomical images (TR/ΔTE/TEeff: 3100/11/33 ms, RARE factor: 8, 29 consecutive slices, slice thickness 0.45 mm, FOV: (16.2 mm)2, resolution: 100 µm2, NA: 2, 2 min 4 s). A stimulated echo acquisition mode (STEAM) sequence was used for spectroscopy following local shimming (MAPSHIM) across a cubic 8 mm3 voxel placed in the striatum (TR/TE/mixing time: 2500 ms/3 ms/10 ms, number of averages (NA): 256, VAPOR water suppression, 10 min 40 s).

MRI Data Analysis

CBF maps were calculated using the Perfusion ASL macro in Paravision 5.1 software via the T1 method using a blood T1 value of 2100 ms and a brain blood partition coefficient of 0.89 mL/g [1,2]. Analysis of the CBF values were done using a custom written Matlab toolbox for nonlinear atlas registration [3] was used to select the CBF slice from the volume and coregister the CBF on the T2 images. Finally T2 and CBF images were transformed into the Allen brain atlas space and the atlas based CBF-values were extracted for all correlating Allen brain atlas structures in both hemispheres. (Release 2013a (MathWorks, Natick, MA, USA) script extracted the CBF maps from Paravision, and used atlas registration and coregistration of CBF maps in the atlas space for striatum and prefrontal cortex). The resulting CBF values were expressed in mL/min/100g.

Tissue preparation and staining procedures

At the conclusion of the experiments, mice were deeply anaesthetized with ketamine and xylazine and perfused through the heart with physiological saline followed by 4% paraformaldehyde, Alexa Fluor® 680 conjugate of WGA, Termofisher, W32465, 3% Gelatin (Sigma-Aldrich, G1890), 1% low melting agarose (Sigma Aldrich A4018) and 0.1% Evans Blue (Sigma Aldrich E2129). Whole brains were scanned with Li-cor (Li-Cor Odyssey-CLx). Subsequently, the brains were post-fixed for 24 hours in 4% PFA, and cryoprotected in 30% sucrose solution before being snap frozen in -40 ºC methylbutane. Tissue was sectioned to 50 µm and stored in cryo-protective solution (1 part ethylene glycol, 1 part glycerine and 2 parts phosphate buffered saline (PBS)) at -20 ºC.

Retina histology

Imunohistochemistochemical analysis of retinal sagittal sections was performed as previously described (Crespo-Garcia et al. PLOS ONE 2018). In short, after fixation of the eyes in 4% PFA and embedding in paraffin, 5um thin sections were stained for H/E, or GFAP (Z0334, DAKO, Hamburg, Germany) or CTBP2 (ab128871, Abcam, Cambridge GB) at 4°C overnight. Subsequently the sections were incubated with fluorescence conjugated secondary antibodies for 1h at RT and nuclei were counterstained with DAPI (Sigma, Taufkirchen, Germany). Images were digitalized using a Zeiss Axio Imager microscope and Zen-Lite 2012 software (Zeiss, Jena, Germany)

References

1. Leithner C, Müller S, Füchtemeier M, et al. Determination of the brain-blood partition coefficient for water in mice using MRI. *J Cereb Blood Flow Metab* 2010; 30: 1821–1824.
2. Dobre MC, Uğurbil K, Marjanska M. Determination of blood longitudinal relaxation time (T1) at high magnetic field strengths. *Magn Reson Imaging* 2007; 25: 733–735.
3. Koch S, Mueller S, Foddis M, et al. Atlas registration for edema-corrected MRI lesion volume in mouse stroke models. *J Cereb Blood Flow Metab* 2017; 271678X17726635.

Legends supplementary figures and tables

FigS1

MCAO and BCCAS models with surgical key features and collateral blood flow during acute ischemia. The blue arrows indicate the direction of the collateral blood flow following the surgery. **A**. Basilar artery (BA) → superior cerebellar artery (SCA) → posterior communicating artery (PcomA) → posterior cerebral artery (PCA). **B.** Basilar artery (BA) → left superior cerebellar artery (SCA) → left posterior communicating artery (PcomA) → left posterior cerebral artery (PCA) and right anterior cerebral artery (ACA) → anterior communicating artery (AcomA) → left anterior cerebral artery (ACA). CCA, common carotid artery, BA, basilar artery, ICA, internal carotid artery, OA, ophthalmic artery.

FigS2

A-B exemple of very prominent PcomA, based on the PcomA/BA diameter ratio measurements both with Evans Blue and WGA stainings. **C-D** Angiotool analysis of microvessel density, average length and anastomoses at the superficial leptomeningeal and cortical and deep gray striatal level. Leptomeningeal and deep microvessels during hypoperfusion. Region of interest has been always kept the same, both in terms of dimensions and brain regions in both hemispheres. Scale bar = 1mm.

FigS3

PcomAs in naive, BCCAS and MCAO mice. In the absence of a pressure gradient in the Circle of Willis, PcomAs (white arrows) are not recruited and appear hypoplstic and subtle, not detectable on MRA. Analogously, basilar artery (BA, red arrow) and PCA (yellow arrows), PcomA affluents and effluents, respectively, display a small diameter (**A**). By contrast, during ischemia, PcomAs become patent, progressively more prominent, and clearly detectable on MRA (**B-D, MRI,** white arrows). **A** Naïve mice, displaying none or non-patent PcomAs. **B-C** BCCAS mice 7 days post-surgery, displaying 2 and 1 prominent PcomAs and BA with increased diameter. **D-E** MCAO mice, 7 wks post-surgery displaying prominent and small left PcomAs. **E** MCAO mice with very subtle PcomAs and markedly increased tortuosity on the left side, barely detectable on the MRA

FigS4

BCCAS MRA showing Circle of Willis and ECA retrograde flow at different time points: pre-surgery, 1 day, 7 days and 7 weeks post-surgery. **A BCCAS mice pre-surgery**. Complete circle of Willis loop (blue arrows) and absence of ECA retrograde flow (yellow arrows). **B** BCCAS 1d post-surgery. Weak MRA intensity in correspondence of ACA-MCA watershed areas (blue arrows). Retrograde flow from ECA (yellow arrows). **C**. BCCAS 7d post-surgery. Collateral flow recruitment and initial hemodynamic recovery of ACA-MCA territories inferable from an increased MRA intensity (blue arrows). **D**. BCCAS 7 weeks post-surgery. CBF recovery and return to the pre-surgery hemodynamic condition, with complete circle of Willis loop with persistence of ECA retrograde flow.

FigS5

BCCAS MRA at day 1: different pattern of ECA retrograde flow (blue arrows): only left ECA retrograde flow associated to contralateral small subcortical lesions corresponding to the right ACA-MCA border zones (**A**); only right ECA retrograde flow associated to contralateral small subcortical lesions, corresponding to the left ACA-MCA watershed areas (**B**) and both left and right ECA retrograde flow associated to no lesions detectable on T2 weighted MRI (**C**). Scale bars: B, D = 1mm; C, E= 0.5mm

FigS6

A-E MRA (**A**), IBA1(**B-C**) and GFAP (**D-E**) staining of a BCCAS mouse displaying no ischemic lesions detectable on MRA but significant microglia and astrocytes activation in both hippocampi and right frontal cortex, 8 days post-surgery. Scale bars represent 1mm (**B**, **D**) and 0.5mm (**C**, **E**)

FigS7

A-C Retina progressive degeneration during subacute and chronic hypoperfusion (8 days and 6 months post-surgery, respectively) in BCCAS mice. **A**. Representative sagittal sections of the retina stained against glial fibrillary acidic protein (GFAP, in green) showing marked gliosis in BCCAS animals both at 8 days (**D8**) and 6 months (**M6**). Sham animals served as control. Nuclei are counterstained with DAPI (blue). Scale bar represents 50 um. **B**. Representative sagittal sections of the retina stained against C-terminal binding protein 2 (CTBP2, in red) showing delocalization and loss of presynaptic protein in the OPL in BCCAS animals, 8 days (**D8**), with a progressive worsening at 6 months (**M6**). Sham animals served as control. Nuclei are counterstained with DAPI (blue). Scale bar represents 50 um. **C**. Representative sagittal sections of the retina, stained with hematoxylin and eosin, displaying significant thinning and atrophy during chronic hypoperfusion (**M6**). Scale bar= 0.5mm

FigS8

MCAO extreme neuroimaging and vascular phenotypes: mice with prominent (**A**) and small (**B, C**) left PcomA. Detailed description in the supplementary

FigS9

Microllateral plasticity in hypoperfused striatum and cortex in MCAO and BCCAS mice. Scale bar represents 0.5mm

FigS10

White matter microvessels in naïve, MCAO and BCCAS mice showing a macroscopically significant reduced density of microvessels in corpus callosum (long dash lines), compared to adjacent gray matter, both for naïve, MCAO and BCCAS mice (**A-E**). Increased microvessel diameter size in white matter in proximity of the ischemic core (blue arrow) (**F, G**)

TableS1

BCCAS lesion volume and percentage of left and right hemisphere affected during acute and subacute hypoperfusion (1-7 days)

TableS2

CBF drop in BCCAS in cortex and striatum during acute and subacute hypoperfusion (1-7 days)

TableS3

Percentage of CBF reduction in BCCAS in cortex and striatum during acute and subacute hypoperfusion (1-7 days)

TableS4

Brain areas mostly affected by ischemic lesions in BCCAS at day 1

TableS5

CBF reduction in left and right hemisphere in MCAO 1 day, 1, 4 and 7 weeks post-surgery

TableS6

Percentage of CBF reduction in MCAO left and right hemisphere at day 1

TableS7

Lesion volume and percentage of left hemisphere affected at day 1 and 7 in MCAO

TableS8

Percentage of brain areas affected in MCAO mice with different PcomA patterns

TableS9

Arteriole diameter in the infarct area of MCAO mice and in naïve mice

TableS10

Microvessel features in MCAO and BCCAS hypoperfused brain areas

TableS11

Leptomeningeal vessel features in MCAO and naïve mice

Fig S1

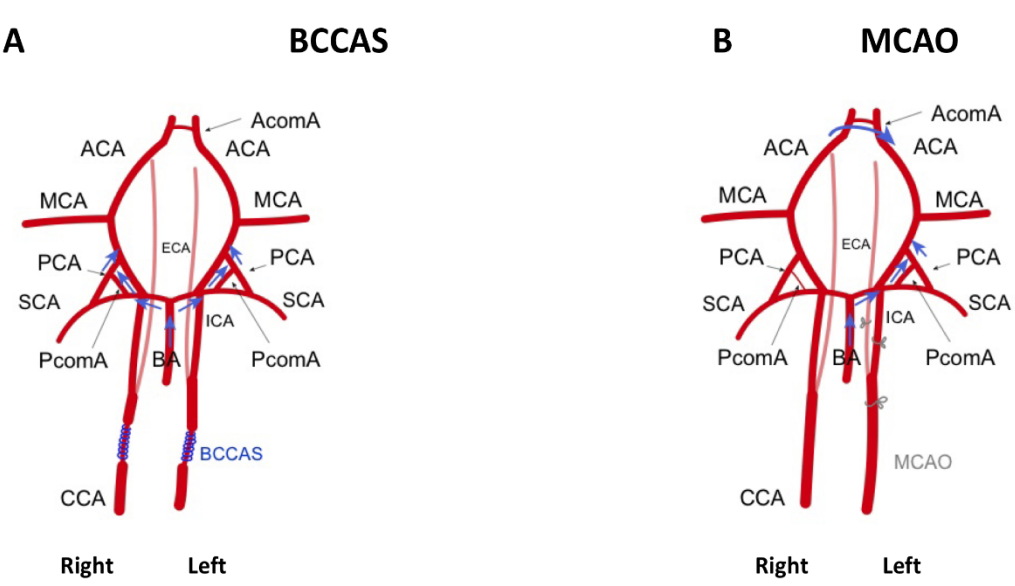
A
BCCAS
AcomA
ACA
ACA
MCA
MCA
ECA
PCA
PCA
SCA
SCA
ICA
PcomA
BA
PcomA
BCCAS
CCA
Right
Left
B
MCAO
AcomA
ACA
ACA
MCA
MCA
ECA
PCA
PCA
SCA
SCA
ICA
PcomA
BA
PcomA
MCAO
CCA
Right
Left

Fig S2

Very prominent PcomA: PcomA>60% BA

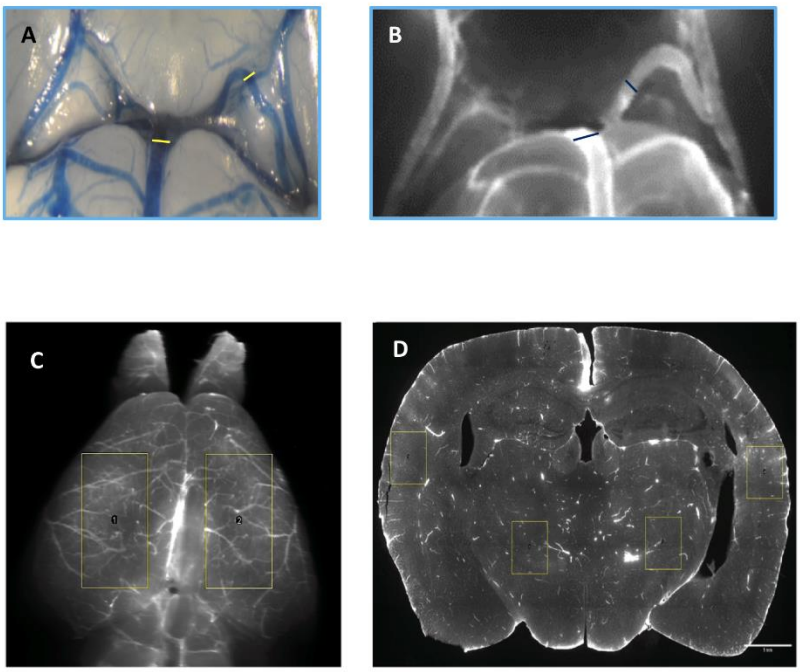

Fig S3

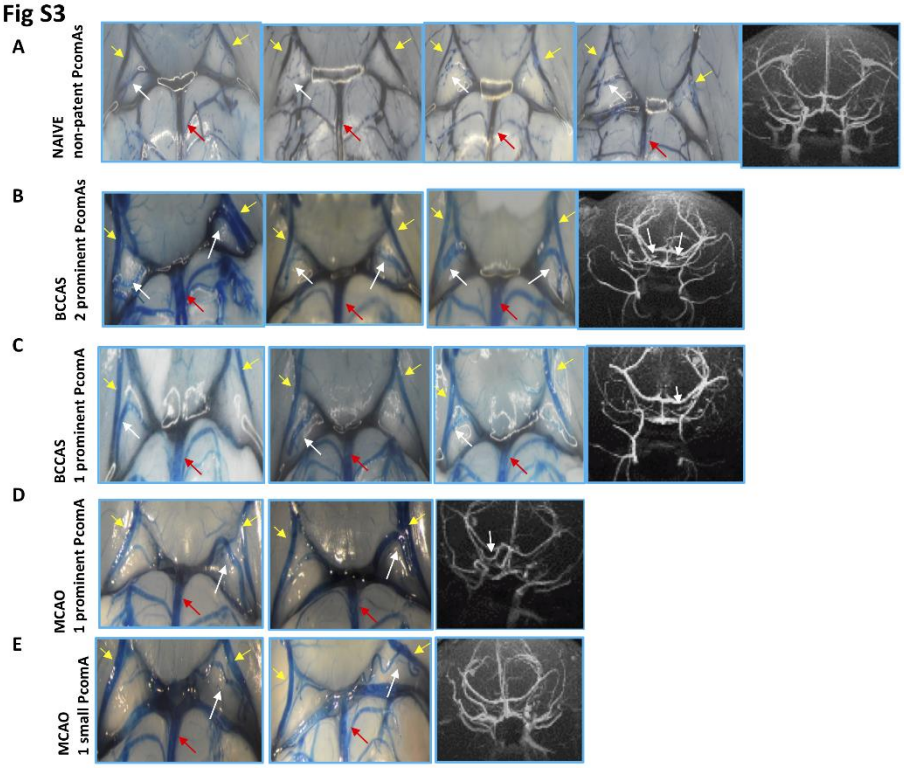
A
NAIVE
non-patent PcomAs
B
BCCAS
2 prominent PcomAs
C
BCCAS
1 prominent PcomA
D
MCAO
1 prominent PcomA
E
MCAO
1 small PcomA

Fig S4

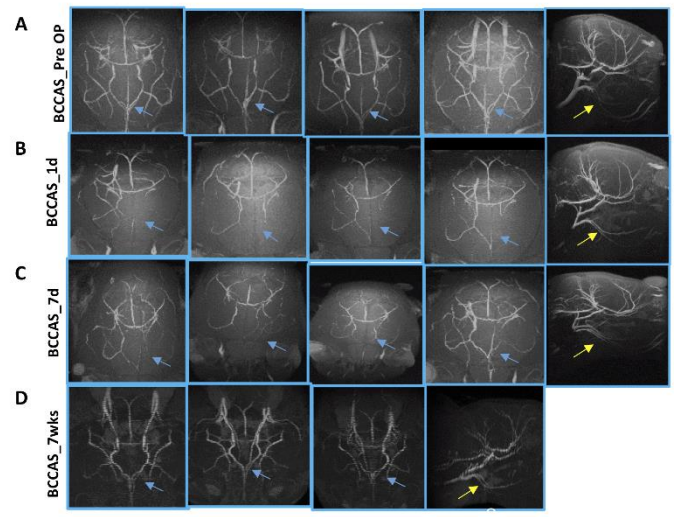
A
BCCAS_Pre OP
B
BCCAS_1d
C
BCCAS_7d
D
BCCAS_7wks

Fig S5

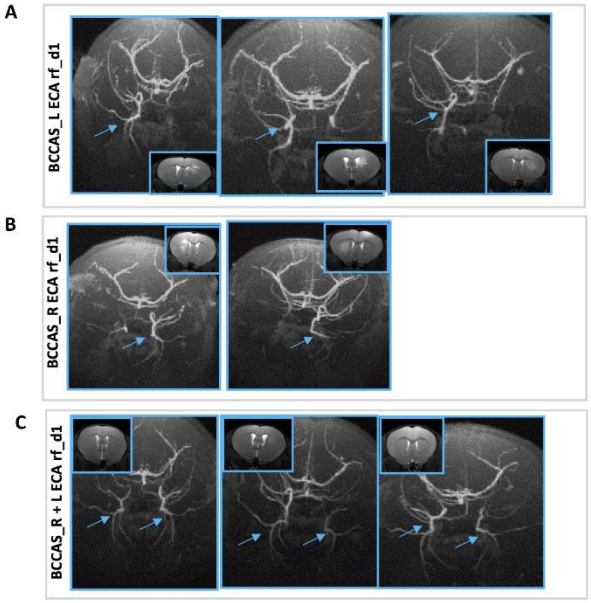

Fig S6

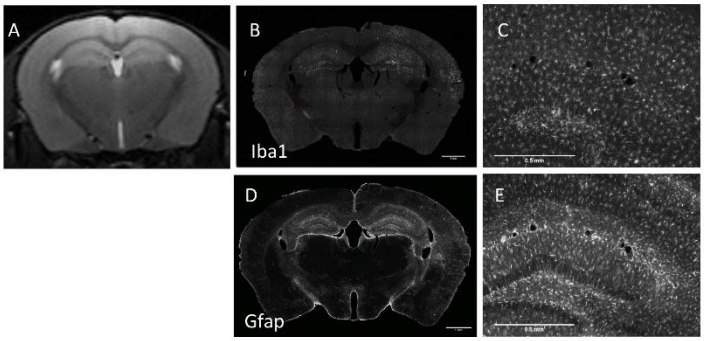
A
B
Iba1
C
D
Gfap
E

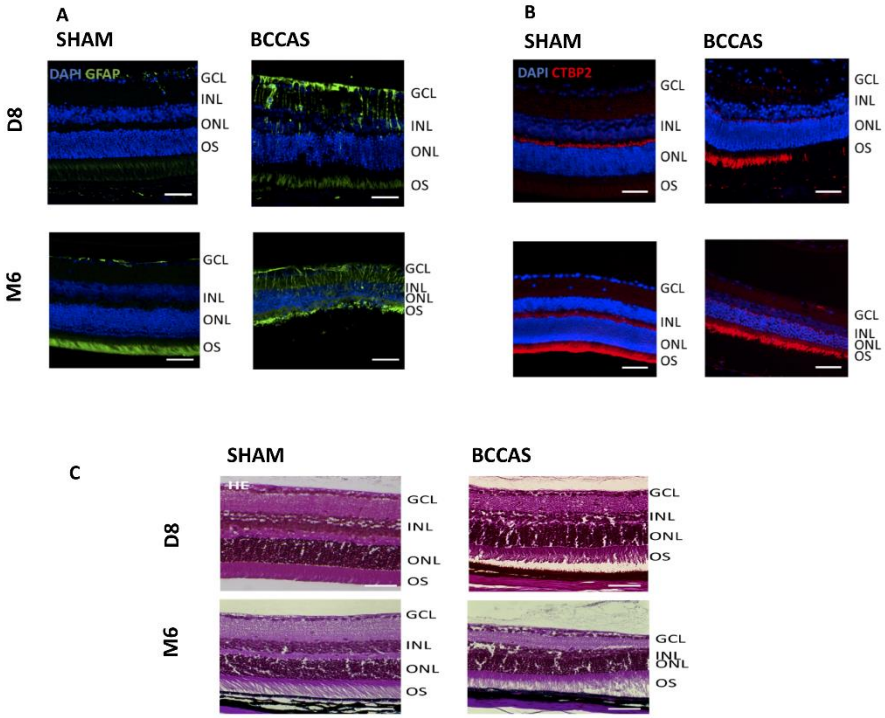
A
SHAM
BCCAS
D8
M6
DAPI GFAP
GCL
INL
ONL
OS
B
SHAM
BCCAS
DAPI CTBP2
C
SHAM
BCCAS
D8
M6
HE

Fig S7

Fig S8

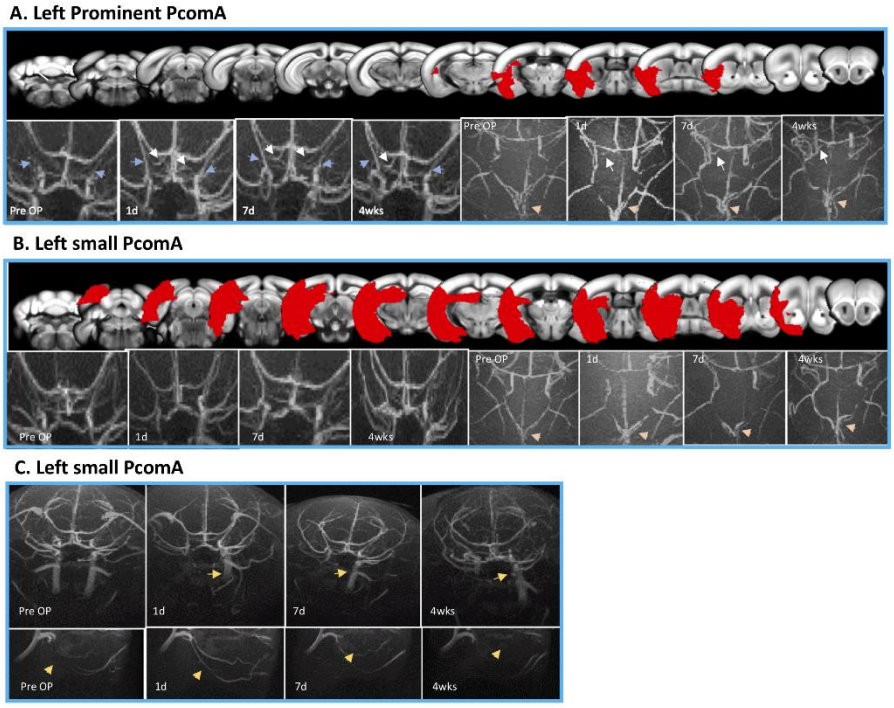
A. Left Prominent PcomA
Pre OP
1d
7d
4wks
B. Left small PcomA
Pre OP
1d
7d
4wks
C. Left small PcomA
Pre OP
1d
7d
4wks

Fig S9

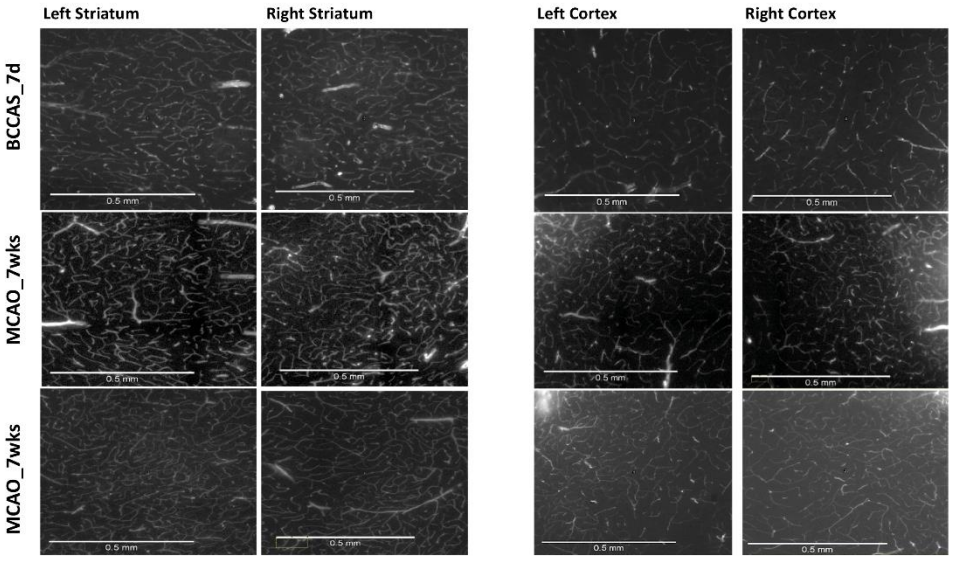
Left Striatum
Right Striatum
Left Cortex
Right Cortex
BCCAS_7d
MCAO_7wks
MCAO_7wks
0.5 mm

Fig S10

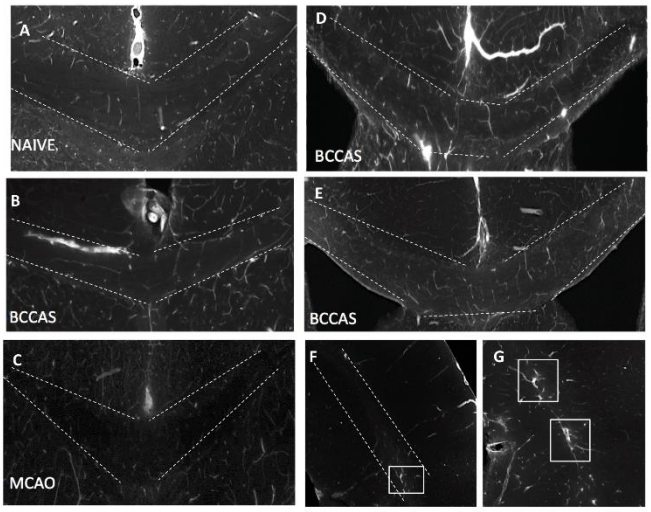

Table S1

MouseID_vascular phenotype	Time	Lesion Volume Left (mm3)	Percentage of Left Hemisphere	Lesion Volume Right (mm3)	Percentage of Right Hemisphere	Time	Lesion Volume Left (mm3)	Percentage of Left Hemisphere	Lesion Volume Right (mm3)	Percentage of Right Hemisphere
BCCAS_1 ECA (L), 2 non-patent PcomAs	day 1	0,147	0%	10,61	4%	day 7	0	0%	3,5	1%
BCCAS_1 ECA (L), no PcomAs	day 1	0	0%	52,9	20%	day 7	/	/	/	/
BCCAS_2 ECAs_1 prominent PcomA (R)	day 1	0	0%	10,57	4%	day 7	0	0%	12,887	5%
BCCAS_1 ECA (L), 1 prominent (R), 1 small (L) PcomAs	day 1	0	0%	9,38	4%	day 7	0	0%	32,762	13%
BCCAS_2 ECAs, 2 prominent PcomAs	day 1	0	0%	10,8	4%	day 7	0	0%	0	0%
BCCAS_1 ECA (L), no PcomAs	day 1	0,042	0%	42,296	16%	day 7	/	/	/	/
BCCAS_2 ECAs, 1 prominent (R) PcomA	day 1	0	0%	0	0%	day 7	0	0%	0	0%
BCCAS_1 prominent PcomA (L)	day 1	0,32	0%	96,63	37%	day 7	/	/	/	/
BCCAS_2 ECAs, 1 prominent (L), 1 small (R) PcomAs	day 1	0	0%	22,57	9%	day 7	0	0%	1,25	0%
BCCAS_2 ECAs, 1 prominent (R), 1 small (L) PcomAs	day 1	21,284	8%	0	0%	day 7	1,109	0%	0	0%
BCCAS_1 ECA (R), 1 prominent (L) PcomA	day 1	8,545	3%	6,986	3%	day 7	84,627	32%	0,001	0%
BCCAS_1 ECA (R), 1 prominent PcomA (R)	day 1	50,358	19%	0	0%	day 7	/	/	/	/
BCCAS_1 ECA (L), 1 prominent PcomA (R)	day 1	0	0%	1,176	0%	day 7	0	0%	33,212	13%
BCCAS_1 ECA (L)_2 prominent PcomAs	day 1	0	0%	0	0%	day 7	0	0%	19,247	7%
BCCAS_2 ECAs, 1 prominent (R), 1 non-patent PcomA	day 1	0	0%	0	0%	day 7	0	0%	0	0%
BCCAS_1 ECA (L)_2 very prominent PcomAs	day 1	0	0%	21,667	8%	day 7	0	0%	7,154	3%
BCCAS_1 ECA (L),no PcomAs	day 1	0	0%	20,227	8%	day 7	/	/	/	/
BCCAS_1 ECA (L), 1 prominent PcomA (R)	day 1	0	0%	12,07	5%	day 7	0,478	0%	47,427	18%
BCCAS_2 ECAs, 1 prominent (R) PcomA	day 1	0	0%	0	0%	day 7	0	0%	2,887	1%
BCCAS_1 ECA (L), 1 prominent (R), 1 small (L) PcomAs	day 1	0	0%	1,15	0%	day 7	0	0%	13,154	5%

Table S2

Mouse.ID_vascular phenotype	Time	CBF_Cx_L	CBF_Cx_R	CBF_S_L	CBF_S_R
BCCAS_1 ECA (L), 2 non-patent PcomAs	0d	122,5151822	126,8046884	118,8884354	107,8328454
BCCAS_1 ECA (L), 2 non-patent PcomAs	1d	15,80999825	8,599138384	31,83154433	19,11489724
BCCAS_1 ECA (L), 2 non-patent PcomAs	7d	16,58669945	23,15701226	24,95434232	31,57716935
BCCAS_2 ECAs_1 prominent PcomA (R)	0d	102,3838066	100,8180672	83,09938819	84,811758
BCCAS_2 ECAs_1 prominent PcomA (R)	1d	49,81267848	18,44921259	40,84048021	22,33278601
BCCAS_2 ECAs_1 prominent PcomA (R)	7d	48,34756302	28,39457039	34,29972463	33,81740931
BCCAS_1 ECA (L), 1 prominent (R), 1 small (L) PcomAs	0d	100,5850698	94,65422142	84,19319033	84,12428289
BCCAS_1 ECA (L), 1 prominent (R), 1 small (L) PcomAs	1d	38,89821156	16,68755184	36,9580093	12,19594067
BCCAS_1 ECA (L), 1 prominent (R), 1 small (L) PcomAs	7d	34,21791671	31,11728145	26,79864966	43,48793622
BCCAS_2 ECAs, 2 prominent PcomAs	0d	148,1978054	119,5375315	101,7579657	101,3710414
BCCAS_2 ECAs, 2 prominent PcomAs	1d	119,1587748	40,91341499	38,51441863	35,50790529
BCCAS_2 ECAs, 2 prominent PcomAs	7d	49,31353771	74,0564812	43,84745201	61,81320127
BCCAS_2 ECAs, 1 prominent (R) PcomA	0d	119,4653261	118,9142491	102,1385652	106,762177
BCCAS_2 ECAs, 1 prominent (R) PcomA	1d	18,43742585	18,3667939	11,84601379	20,57022758
BCCAS_2 ECAs, 1 prominent (R) PcomA	7d	27,15245614	25,93613271	27,23285421	25,98505416
BCCAS_2 ECAs, 1 prominent (L), 1 small (R) PcomAs	0d	96,30399541	92,85534639	83,38072698	79,593287
BCCAS_2 ECAs, 1 prominent (L), 1 small (R) PcomAs	1d	11,244445	16,76109829	24,81191087	20,32340446
BCCAS_2 ECAs, 1 prominent (L), 1 small (R) PcomAs	7d	47,50977888	37,25285076	50,39292132	24,51169131
BCCAS_2 ECAs, 1 prominent (R), 1 small (L) PcomAs	0d	105,3243051	102,2613978	95,99867676	86,93208341
BCCAS_2 ECAs, 1 prominent (R), 1 small (L) PcomAs	1d	20,24317276	31,50885495	27,67283483	30,76080368
BCCAS_2 ECAs, 1 prominent (R), 1 small (L) PcomAs	7d	29,725681	22,30161511	35,87385678	26,22280155
BCCAS_1 ECA (R), 1 prominent (L) PcomA	0d	105,9159861	115,5616856	93,46209257	91,84569293
BCCAS_1 ECA (R), 1 prominent (L) PcomA	1d	8,548924982	37,63401024	20,33453735	42,68682635
BCCAS_1 ECA (R), 1 prominent (L) PcomA	7d	25,27066323	43,56697057	33,86099161	56,88317673
BCCAS_1 ECA (L), 1 prominent PcomA (R)	0d	150,948701	162,7002073	124,7177342	131,4578272
BCCAS_1 ECA (L), 1 prominent PcomA (R)	1d	26,57978798	6,420303985	36,03173341	22,8710745
BCCAS_1 ECA (L), 1 prominent PcomA (R)	7d	34,6706141	30,26654468	35,60939813	28,60813856
BCCAS_1 ECA (L)_2 prominent PcomAs	0d	123,1388995	134,2918251	115,1781724	105,0895912
BCCAS_1 ECA (L)_2 prominent PcomAs	1d	46,59561613	9,356240452	41,25656616	13,2522298
BCCAS_1 ECA (L)_2 prominent PcomAs	7d	35,78513463	35,47261824	39,44967665	39,18432408
BCCAS_2 ECAs, 1 prominent (R), 1 non-patent PcomA	0d	140,6842408	143,871155	119,5649627	121,8189768
BCCAS_2 ECAs, 1 prominent (R), 1 non-patent PcomA	1d	50,50360711	57,07628213	59,10361578	52,15501891
BCCAS_2 ECAs, 1 prominent (R), 1 non-patent PcomA	7d	23,14678341	11,00366503	28,86077124	14,74550895
BCCAS_1 ECA (L)_2 very prominent PcomAs	0d	145,5783979	147,9625691	126,5684181	123,9633927
BCCAS_1 ECA (L)_2 very prominent PcomAs	1d	33,2317219	16,784005	28,89517024	17,25487531
BCCAS_1 ECA (L)_2 very prominent PcomAs	7d	27,62065712	29,50330075	31,64862085	54,76417538
BCCAS_1 ECA (L),no PcomAs	0d	168,0959761	170,1882061	138,9689797	135,6249711
BCCAS_1 ECA (L),no PcomAs	1d	20,41111115	8,628693719	33,39621499	13,58930286
BCCAS_1 ECA (L),no PcomAs	7d	0	0	0	0
BCCAS_1 ECA (L), 1 prominent PcomA (R)	0d	110,9645619	111,4418065	117,0161945	117,1090963
BCCAS_1 ECA (L), 1 prominent PcomA (R)	1d	19,4037094	11,31069992	29,95191682	20,84810936
BCCAS_1 ECA (L), 1 prominent PcomA (R)	7d	23,05738228	21,0720244	23,63616542	39,14571221
BCCAS_2 ECAs, 1 prominent (R) PcomA	0d	151,1678728	156,5888276	131,3001053	126,8715154
BCCAS_2 ECAs, 1 prominent (R) PcomA	1d	24,39315253	12,89354549	26,27374452	13,66020014
BCCAS_2 ECAs, 1 prominent (R) PcomA	7d	41,21464798	48,53516517	37,56716301	42,34493351
BCCAS_1 ECA (L), 1 prominent (R), 1 small (L) PcomAs	0d	142,9266555	142,1960638	119,6681323	117,5792076
BCCAS_1 ECA (L), 1 prominent (R), 1 small (L) PcomAs	1d	40,99092955	10,59265714	44,66482211	22,73320437
BCCAS_1 ECA (L), 1 prominent (R), 1 small (L) PcomAs	7d	83,23086078	67,77553327	72,36598397	56,07105418

Table S3

Mouse.ID	Time	%CBF_reduction_Cx_L	%CBF_reduction_Cx_R	%CBF_reduction_S_L	%CBF_reduction_S_R
BCCAS_1 ECA (L), 2 non-patent PcomAs	d0-d1	86,51	93,21	73,22	82,26
BCCAS_03	d0-d1	93,44	99,12	76,8	91,73
BCCAS_2 ECAs_1 prominent PcomA (R)	d0-d1	51,34	81,69	50,84	73,65
BCCAS_1 ECA (L), 1 prominent (R), 1 small (L) PcomAs	d0-d1	61,32	82,36	56,097	85,51
BCCAS_2 ECAs, 2 prominent PcomAs	d0-d1	19,56	65,77	62,14	64,96
BCCAS_10	d0-d1	97,09	98,59	83,81	94,57
BCCAS_2 ECAs, 1 prominent (R) PcomA	d0-d1	84,54	84,54	88,51	80,73
BCCAS_2 ECAs, 1 prominent (L), 1 small (R) PcomAs	d0-d1	88,26	81,84	70,23%	74,45
BCCAS_2 ECAs, 1 prominent (R), 1 small (L) PcomAs	d0-d1	80,77	69,18	71,16	64,61
BCCAS_1 ECA (R), 1 prominent (L) PcomA	d0-d1	91,92	67,4	78,23	53,51
BCCAS_20	d0-d1	98,02	83,61	88,87	73,3
BCCAS_1 ECA (L), 1 prominent PcomA (R)	d0-d1	82,38	96,04	71,1	82,12
BCCAS_1 ECA (L)_2 prominent PcomAs	d0-d1	62,15	93,02	64,17	87,38
BCCAS_2 ECAs, 1 prominent (R), 1 non-patent PcomA	d0-d1	64,1	60,32	50,56	57,18
BCCAS_1 ECA (L)_2 very prominent PcomAs	d0-d1	77,16	88,65	77,16	86,07
BCCAS_1 ECA (L),no PcomAs	d0-d1	87,85	94,92	75,96	89,95
BCCAS_1 ECA (L), 1 prominent PcomA (R)	d0-d1	82,51	90,2	87,06	82,19
BCCAS_2 ECAs, 1 prominent (R) PcomA	d0-d1	83,86	91,76	79,96	89
BCCAS_1 ECA (L), 1 prominent (R), 1 small (L) PcomAs	d0-d1	71,31	92,54	62,67	80,66
BCCAS_1 ECA (L), 2 non-patent PcomAs	d0-d7	86,46	81,7	79	70,72
BCCAS_03	d0-d7	NA	NA	NA	NA
BCCAS_2 ECAs_1 prominent PcomA (R)	d0-d7	52,74	71,83	59	60
BCCAS_1 ECA (L), 1 prominent (R), 1 small (L) PcomAs	d0-d7	65,98	67,13	68,17	47,55
BCCAS_2 ECAs, 2 prominent PcomAs	d0-d7	66,72	38	56,9	39
BCCAS_10	d0-d7	NA	NA	NA	NA
BCCAS_2 ECAs, 1 prominent (R) PcomA	d0-d7	77,27	78,79	73,33	75,47

BCCAS_2 ECAs, 1 prominent (L), 1 small (R) PcomAs	d0-d7	50,67	59,8	39,5	69,18
BCCAS_2 ECAs, 1 prominent (R), 1 small (L) PcomAs	d0-d7	71,78	78,39	62,63	69,8
BCCAS_1 ECA (R), 1 prominent (L) PcomA	d0-d7	75,5	62,6	63,46	38
BCCAS_20	d0-d7	NA	NA	NA	NA
BCCAS_1 ECA (L), 1 prominent PcomA (R)	d0-d7	77	81,48	71,4	78,2
BCCAS_1 ECA (L)_2 prominent PcomAs	d0-d7	70,9	73,74	65,75	62,7
BCCAS_2 ECAs, 1 prominent (R), 1 non-patent PcomA	d0-d7	83,5	92,3	75,27	87,8
BCCAS_1 ECA (L)_2 very prominent PcomAs	d0-d7	80,6	80,27	74,27	55,7
BCCAS_1 ECA (L),no PcomAs	d0-d7	NA	NA	NA	NA
BCCAS_1 ECA (L), 1 prominent PcomA (R)	d0-d7	78,7	81	79,8	66,63
BCCAS_2 ECAs, 1 prominent (R) PcomA	d0-d7	72,7	68,97	71,4	66,66
BCCAS_1 ECA (L), 1 prominent (R), 1 small (L) PcomAs	d0-d7	41,28	52,4	39,5	52,62

Table S4

Brain region	Time	Percentage affected
Cerebral cortex_L	0-1d	0
Cerebral cortex_L	0-1d	0
Cerebral cortex_L	0-1d	0
Cerebral cortex_L	0-1d	0
Cerebral cortex_L	0-1d	0
Cerebral cortex_L	0-1d	0
Cerebral cortex_L	0-1d	0
Cerebral cortex_L	0-1d	0
Cerebral cortex_L	0-1d	0
Cerebral cortex_L	0-1d	12
Cerebral cortex_L	0-1d	1
Cerebral cortex_L	0-1d	33
Cerebral cortex_L	0-1d	0
Cerebral cortex_L	0-1d	0
Cerebral cortex_L	0-1d	0
Cerebral cortex_L	0-1d	0
Cerebral cortex_L	0-1d	0
Cerebral cortex_L	0-1d	0
Cerebral cortex_L	0-1d	0
Cerebral cortex_L	0-1d	0
Cerebral cortex_R	0-1d	7
Cerebral cortex_R	0-1d	5
Cerebral cortex_R	0-1d	34
Cerebral cortex_R	0-1d	3
Cerebral cortex_R	0-1d	5
Cerebral cortex_R	0-1d	30
Cerebral cortex_R	0-1d	0

Cerebral cortex_R	0-1d	60
Cerebral cortex_R	0-1d	13
Cerebral cortex_R	0-1d	0
Cerebral cortex_R	0-1d	5
Cerebral cortex_R	0-1d	0
Cerebral cortex_R	0-1d	0
Cerebral cortex_R	0-1d	0
Cerebral cortex_R	0-1d	0
Cerebral cortex_R	0-1d	13
Cerebral cortex_R	0-1d	13
Cerebral cortex_R	0-1d	6
Cerebral cortex_R	0-1d	0
Cerebral cortex_R	0-1d	0
Striatum_L	0-1d	0
Striatum_L	0-1d	0
Striatum_L	0-1d	0
Striatum_L	0-1d	0
Striatum_L	0-1d	0
Striatum_L	0-1d	0
Striatum_L	0-1d	0
Striatum_L	0-1d	0
Striatum_L	0-1d	0
Striatum_L	0-1d	26
Striatum_L	0-1d	35
Striatum_L	0-1d	25
Striatum_L	0-1d	0
Striatum_L	0-1d	0
Striatum_L	0-1d	0
Striatum_L	0-1d	0
Striatum_L	0-1d	0
Striatum_L	0-1d	0
Striatum_L	0-1d	0
Striatum_L	0-1d	0
Striatum_R	0-1d	7
Striatum_R	0-1d	16
Striatum_R	0-1d	34
Striatum_R	0-1d	22
Striatum_R	0-1d	20
Striatum_R	0-1d	17
Striatum_R	0-1d	0
Striatum_R	0-1d	61
Striatum_R	0-1d	20
Striatum_R	0-1d	0
Striatum_R	0-1d	0
Striatum_R	0-1d	0
Striatum_R	0-1d	3
Striatum_R	0-1d	0
Striatum_R	0-1d	0
Striatum_R	0-1d	21
Striatum_R	0-1d	10
Striatum_R	0-1d	21
Striatum_R	0-1d	0
Striatum_R	0-1d	5
corpus callosum_L	0-1d	0
corpus callosum_L	0-1d	0
corpus callosum_L	0-1d	0
corpus callosum_L	0-1d	0
corpus callosum_L	0-1d	0

corpus callosum_L	0-1d	0
corpus callosum_L	0-1d	0
corpus callosum_L	0-1d	0
corpus callosum_L	0-1d	0
corpus callosum_L	0-1d	12
corpus callosum_L	0-1d	8
corpus callosum_L	0-1d	45
corpus callosum_L	0-1d	0
corpus callosum_L	0-1d	0
corpus callosum_L	0-1d	0
corpus callosum_L	0-1d	0
corpus callosum_L	0-1d	0
corpus callosum_L	0-1d	0
corpus callosum_L	0-1d	0
corpus callosum_R	0-1d	21
corpus callosum_R	0-1d	18
corpus callosum_R	0-1d	50
corpus callosum_R	0-1d	21
corpus callosum_R	0-1d	10
corpus callosum_R	0-1d	30
corpus callosum_R	0-1d	0
corpus callosum_R	0-1d	58
corpus callosum_R	0-1d	18
corpus callosum_R	0-1d	0
corpus callosum_R	0-1d	0
corpus callosum_R	0-1d	0
corpus callosum_R	0-1d	0
corpus callosum_R	0-1d	0
corpus callosum_R	0-1d	0
corpus callosum_R	0-1d	8
corpus callosum_R	0-1d	29
corpus callosum_R	0-1d	14
corpus callosum_R	0-1d	0
corpus callosum_R	0-1d	2

Table S5

Mouse.ID_Left PcomA size	Time	CBF.L.Cx	CBF.R.Cx	CBF_L_S	CBF_R_S
MCAO_small PcomA	0d	121,7217438	134,8766681	122,9761684	117,1312997
MCAO_small PcomA	1d	28,11460357	86,02938802	23,57986906	77,77926985
MCAO_small PcomA	w1	54,38543794	22,95552849	72,17551682	27,34018097
MCAO_small PcomA	w4	157,2796521	147,0541602	126,2804012	129,9610161
MCAO_small PcomA	w7	133,6648216	130,8575839	121,8730259	120,0237001
MCAO_prominent PcomA	0d	91,89100813	87,54875419	80,36110607	83,92087564
MCAO_prominent PcomA	1d	71,67986638	151,7484785	36,88779875	121,7840909
MCAO_prominent PcomA	w1	113,6189911	170,3991775	0	133,728953
MCAO_prominent PcomA	w4	132,0771617	154,3481298	107,3513106	128,0006119
MCAO_prominent PcomA	w7	119,1819764	140,2194457	112,1499883	118,7902366
MCAO_prominent PcomA	0d	79,64408888	154,1177827	83,58249192	132,8262835
MCAO_prominent PcomA	1d	35,13595138	89,88345149	31,82496254	88,36865303
MCAO_prominent PcomA	w1	105,4804127	142,2192799	83,0250103	118,3368802
MCAO_prominent PcomA	w4	90,6257627	89,17967317	79,01271079	100,7622792
MCAO_prominent PcomA	w7	146,3542814	146,6366963	111,2093674	133,7403165
MCAO_prominent PcomA	0d	119,1587748	119,5375315	101,7579657	101,3710414
MCAO_prominent PcomA	1d	70,18400005	132,0139974	48,87765355	125,8893253

MCAO_prominent PcomA	w1	119,2303177	166,2346609	87,24550809	128,9586508
MCAO_prominent PcomA	w4	117,8818366	136,9686466	112,9045791	118,2937734
MCAO_prominent PcomA	w7	99,36974484	128,936467	99,05773658	114,4640201
Sham1	0d	119,4653261	118,9142491	102,1385652	106,762177
Sham1	1d	95,40773809	165,3733118	86,77067779	135,8055664
Sham1	w1	68,80468015	127,1829102	66,21255324	105,1416849
Sham1	w4	87,30362146	132,6185576	56,38629951	107,9326888
Sham1	w7	101,4382349	141,9378982	74,21481655	113,229796
MCAO_small PcomA	0d	109,1558396	105,6512367	92,69781618	79,96049683
MCAO_small PcomA	1d	0	0	0	0
MCAO_small PcomA	w1	119,6398383	183,7070966	103,0997559	145,4374715
MCAO_small PcomA	w4	143,4835418	170,123128	137,9077555	129,6729223
MCAO_small PcomA	w7	130,329132	153,0085083	113,0766475	120,935117
MCAO_prominent PcomA	0d	135,3999529	143,6141366	113,3120275	110,6217667
MCAO_prominent PcomA	1d	49,80093722	117,8356514	32,40303897	93,83683181
MCAO_prominent PcomA	w1	104,1966553	154,2536126	84,35959741	138,8184953
MCAO_prominent PcomA	w4	120,2369094	154,9890631	133,4563288	117,1103254
MCAO_prominent PcomA	w7	123,5163482	149,0102428	122,7696109	124,2652151
MCAO_prominent PcomA	0d	141,0751801	151,2674909	117,1686339	126,3095457
MCAO_prominent PcomA	1d	62,60551936	112,8711947	58,36682414	118,2665262
MCAO_prominent PcomA	w1	89,4910837	144,667316	65,98567942	120,8872173
MCAO_prominent PcomA	w4	125,3777166	155,5320208	96,87818551	134,110661
MCAO_prominent PcomA	w7	119,3147637	136,091236	90,15111209	124,05892
MCAO_prominent PcomA	0d	159,6188021	163,0713475	125,4221499	126,1275405
MCAO_prominent PcomA	1d	72,04860286	115,5982871	57,68180814	121,0446762
MCAO_prominent PcomA	w1	113,4569191	157,3518266	101,4835062	127,4698746
MCAO_prominent PcomA	w4	131,5005995	148,5281889	104,4503006	118,6542149
MCAO_prominent PcomA	w7	164,4916357	172,5210105	129,6684647	138,3786645
MCAO_very prominent PcomA	0d	136,9510057	142,846421	115,5675102	116,8556913
MCAO_very prominent PcomA	1d	71,58856537	130,0644248	67,74080225	110,9469922
MCAO_very prominent PcomA	w1	90,94006188	125,0471314	79,2300916	113,3440965
MCAO_very prominent PcomA	w4	93,48691981	130,5689666	89,04324161	109,774079
MCAO_very prominent PcomA	w7	0	0	0	0
MCAO_small PcomA	0d	167,463899	172,3423476	132,3825998	135,6736347
MCAO_small PcomA	1d	35,34085609	106,9577445	25,18028777	101,3700067
MCAO_small PcomA	w1	125,6495675	179,6539852	81,0460181	138,0671222
MCAO_small PcomA	w4	179,2040424	206,1029775	182,4631331	161,030311
MCAO_small PcomA	w7	158,2204011	193,6994786	157,657007	154,1977321

Table S6

Mouse.ID_Left PcomA size	Time	%CBF_reduction_Cx_L	%CBF_reduction_Cx_R	%CBF_reduction_S_L	%CBF_reduction_S_R
MCAO_small PcomA	d0-d1	76,89	36,21	80,82	33,59
MCAO_small PcomA	d0-d1	78,89	37,93	80,97	25,28
MCAO_prominent PcomA	d0-d1	21,99	NA	54,09	NA
MCAO_prominent PcomA	d0-d1	55,87	41,67	61,91	33,46
MCAO_prominent PcomA	d0-d1	41,09	NA	51,96	NA
MCAO_prominent PcomA	d0-d1	63,21	17,94	71,39	15,16

MCAO_prominent PcomA	d0-d1	55,61	25,37	50,18	6,36
MCAO_prominent PcomA	d0-d1	54,86	29,1	54	4
MCAO_very prominent PcomA	d0-d1	47,72	8,94	41,37	5

Table S7

Mouse_ID_Left PcomA size	Time	Lesion Volume corr (mm3)	Percentage of Left Hemisphere
MCAO_very prominent PcomA	day 1	13,39714495	5%
MCAO_prominent PcomA	day 1	20,02939958	8%
MCAO_prominent PcomA	day 1	23,08122521	9%
MCAO_prominent PcomA	day 1	24,89129654	9%
MCAO_prominent PcomA	day 1	28,77980789	11%
MCAO_prominent PcomA	day 1	29,23733173	11%
MCAO_prominent PcomA	day 1	38,43306202	15%
MCAO_small PcomA	day 1	65,39954876	25%
MCAO_small PcomA	day 1	78,11740365	29%
MCAO_small PcomA	day 1	85,14236361	32%
MCAO_small PcomA	day 1	89,2053737	34%
MCAO_very prominent PcomA	day 7	2,230229627	1%
MCAO_prominent PcomA	day 7	3,343831967	1%
MCAO_prominent PcomA	day 7	11,71405527	4%
MCAO_prominent PcomA	day 7	13,701572	5%
MCAO_prominent PcomA	day 7	13,85040924	5%
MCAO_prominent PcomA	day 7	15,83031419	6%
MCAO_prominent PcomA	day 7	22,3526425	8%
MCAO_small PcomA	day 7	42,40507117	16%
MCAO_small PcomA	day 7	68,47733648	26%
MCAO_small PcomA	day 7	69,87355765	26%

Table S8

Left PcomA size	Brain region Left Hemisphere	Percentage affected
1_small	Cortex	50
1_small	Striatum	70
1_small	Hippocampus	80
1_small	Orbital cortex	2
1_small	Cerebellum	0,001
2_prominent	Cortex	22
2_prominent	Striatum	48

2_prominent	Hippocampus	7
2_prominent	Cortex	14
2_prominent	Striatum	54
2_prominent	Hippocampus	4
2_prominent	Orbital cortex	1
2_prominent	Cortex	12
2_prominent	Striatum	30
2_prominent	Hippocampus	1
2_prominent	Cortex	14
2_prominent	Striatum	53
2_prominent	Hippocampus	1
3_very prominent	Cortex	7
3_very prominent	Striatum	24
1_small	Cortex	42
1_small	Striatum	67
1_small	Hippocampus	76
1_small	Cerebellum	0,2
2_prominent	Cortex	12
2_prominent	Striatum	38
2_prominent	Hippocampus	1
2_prominent	Cortex	12
2_prominent	Striatum	54
1_small	Cortex	60
1_small	Striatum	60
1_small	Hippocampus	95
1_small	Orbital cortex	9
1_small	Cerebellum	0,13
1_small	Cortex	38
1_small	Striatum	77
1_small	Hippocampus	72
1_small	Orbital cortex	2

Table S9

Mouse.ID	**Striatal largest arteriole diameter (mm)**							
NAIVE	0.03651	0.02573	0.01574					
BCCAS_infarct area	0.02830	0.02655	0.02053	0.01749	0.01796			
BCCAS_infarct area	0.05344	0.02398	0.02865	0.02452				
MCAO_infarct area	0.02951	0.03514	0.02725	0.03191	0.01572	0.01503	0.03022	0.02873

Table S10

Mouse.ID	Image Name	Junctions density	Average Vessels Length	Total Number of End Points
naïve	cortex_Left	538,3704897	0,049847623	1088
naïve	cortex_Right	408,6903821	0,039334495	1175
naïve	striatum_Left	355,6721503	0,036566375	1164
naïve	striatum_Right	391,0079025	0,042796819	1104
BCCAS_1	cortex_Left	522,4351129	0,055807835	1002
BCCAS_1	cortex_Right	616,5044471	0,058832959	1057
BCCAS_1	striatum_Left	692,9458399	0,093067768	791
BCCAS_1	striatum_Right	634,7130674	0,064552666	994
BCCAS_2	cortex_Left	548,863401	0,071661121	884
BCCAS_2	cortex_Right	658,5747613	0,063180476	1044
BCCAS_2	striatum_Left	548,2891093	0,071187674	895
BCCAS_2	striatum_Right	616,0381077	0,076430543	875
BCCAS_4	cortex_Left	360,6388728	0,046694139	970
BCCAS_4	cortex_Right	394,7299786	0,040909783	1120
BCCAS_4	striatum_Left	348,4005167	0,061089738	806
BCCAS_4	striatum_Right	303,898082	0,058197479	785
MCAO_1	cortex_Left	658,9182335	0,070574473	973
MCAO_1	cortex_Right	562,9044029	0,062687072	1009
MCAO_1	striatum_Left	623,4726576	0,092521882	768
MCAO_1	striatum_Right	564,6675492	0,090903854	746
MCAO_2	cortex_Left	NA	NA	671
MCAO_2	cortex_Right	233,9091131	0,041284494	737
MCAO_2	striatum_Left	472,3904296	0,060927978	904
MCAO_2	striatum_Right	552,3762872	0,061035782	970
MCAO_3	cortex_Left	676,8706775	0,067844597	1022
MCAO_3	cortex_Right	454,6780947	0,057019713	936
MCAO_3	striatum_Left	774,2579954	0,084993157	936
MCAO_3	striatum_Right	380,1742253	0,061629953	825

Table S11

Image Name	Vessels percentage area	Total Number of Junctions	Average Vessels Length
MCAO_1_left_Leptomeningeal v	37,84502066	99	95,68626827
MCAO_1_right_Leptomeningeal v	36,46495324	85	83,08071571
MCAO_2_left_Leptomeningeal v	37,12607738	84	87,46316817
MCAO_2_right_Leptomeningeal v	36,01516261	94	65,77021257
MCAO_4_left_Leptomeningeal v	37,59026701	86	109,7156665
MCAO_4_right_Leptomeningeal v	38,70093985	91	104,8101798
MCAO_6_left_Leptomeningeal v	41,43978119	176	163,7828147
MCAO_6_right_Leptomeningeal v	41,78779508	149	143,361486
MCAO_7_left_Leptomeningeal v	46,50272828	375	186,7528486
MCAO_7_right_Leptomeningeal v	48,09327241	407	356,4544359
MCAO_8_left_Leptomeningeal v	38,5719458	108	81,1014878
MCAO_8_right_Leptomeningeal v	39,13602043	113	88,76021837
MCAO_9_left_Leptomeningeal v	48,45307609	356	231,9044094
MCAO_9_right_Leptomeningeal v	49,57505422	340	236,5029897
MCAO_10_left_Leptomeningeal v	44,53095558	343	153,6039238
MCAO_10_right_Leptomeningeal v	46,23538239	393	149,4258428
MCAO_11_left_Leptomeningeal v	52,98720405	766	348,4308786

MCAO_11_right_Leptomeningeal v	51,880023	721	380,5143175
MCAO_12_left_Leptomeningeal v	48,25368554	571	170,4217349
MCAO_12_right_Leptomeningeal v	51,34258546	646	276,4347156
MCAO_13_left_Leptomeningeal v	51,13976663	732	258,1223597
MCAO_13_right_Leptomeningeal v	44,77579624	708	229,3120222
MCAO_14_left_Leptomeningeal v	43,12752506	412	257,1447909
MCAO_14_right_Leptomeningeal v	55,61812973	751	974,3970818
MCAO_16_left_Leptomeningeal v	46,73768654	435	190,1541202
MCAO_16_right_Leptomeningeal v	48,75711723	488	247,2762852
MCAO_17_left_Leptomeningeal v	48,58739808	497	247,7346537
MCAO_17_right_Leptomeningeal v	47,31696907	434	165,9395078
NAIVE_16_left_Leptomeningeal v	39,75546113	109	128,7679384
NAIVE_16_right_Leptomeningeal v	39,80904229	79	101,5077038
NAIVE_17_left_Leptomeningeal v	42,167035	123	112,1555254
NAIVE_17_right_Leptomeningeal v	40,39368916	115	97,21504817